Lithos 200–201 (2014) 157–168

Contents lists available at ScienceDirect

Lithos

journal homepage: www.elsevier.com/locate/lithos

Geochronology and geochemistry of the Sangri Group Volcanic Rocks, Southern Lhasa Terrane: Implications for the early subduction history of the Neo-Tethys and Gangdese Magmatic Arc

Zhi-Qiang Kang [a,b,c], Ji-Feng Xu [d,*], Simon A. Wilde [c], Zuo-Hai Feng [a], Jian-Lin Chen [d], Bao-Di Wang [e], Wen-Chun Fu [a], Hui-Bin Pan [a]

[a] School of Earth Science and Guangxi Key Laboratory of Hidden Metallic Ore Deposits Exploration, Guilin University of Technology, Guilin, 541004, China
[b] State Key Laboratory of Ore Geochemistry, Institute of Geochemistry, Chinese Academy of Sciences, Guiyang, 550002, China
[c] The Institute for Geoscience Research (TIGeR), Curtin University, Perth, WA 6845, Australia
[d] Key Laboratory of Isotope Geochronology and Geochemistry, Guangzhou Institute of Geochemistry, Chinese Academy of Sciences, Guangzhou, 510640, China
[e] Chengdu Institute of Geology and Mineral Resources, Chengdu, 610081, China

ARTICLE INFO

Article history:
Received 11 December 2013
Accepted 26 April 2014
Available online 9 May 2014

Keywords:
Volcanic rocks
Bima Formation
Sangri Group
Neo-Tethys
Gangdese magmatic arc
Tibet

ABSTRACT

The Sangri Group volcanic rocks are distributed along the southern margin of the Lhasa Terrane on the northern side of the Indus-Yarlung Zangbo suture zone. This Group consists of the Mamuxia and Bima formations and has long been considered to be Late Jurassic to Early Cretaceous in age. In this paper, we report for the first time zircon LA-ICPMS U-Pb ages, whole-rock major and trace element geochemistry, as well as Sr-Nd isotope data of the Bima Formation volcanic rocks in the Sangri County, Tibet. Two samples collected from the Bima Formation volcanic rocks yield zircon U-Pb ages of 195 ± 3 Ma and 189 ± 3 Ma, respectively. These data suggest that the Bima Formation volcanic rocks formed during the Early Jurassic rather than the Late Jurassic-Early Cretaceous as previously reported. The volcanic rocks of the Bima Formation are dominantly composed of basalt and andesite that are enriched in LILEs and LREEs, but depleted in HFSEs, showing typical characteristics of arc volcanic rocks. They also show positive ε_{Nd} (t) (+4.09 to +7.02) values and low initial $^{87}Sr/^{86}Sr$ (0.7032 to 0.7050) ratios, similar to the MORB of the Indus-Yarlung Zangbo ophiolites, indicating that the Bima Formation volcanic rocks were derived from a depleted mantle wedge. The magmas subsequently experienced juvenile crust contamination and fractional crystallization during ascent. Geochemical features of magmas of the Bima Formation volcanic rocks are interpreted to be generated by the northward subduction of Neo-Tethys beneath the southern Lhasa Terrane as early as ~195 Ma. Coeval with a large volume of Late Triassic-Early Jurassic felsic intrusions within the Gangdese arc, the Gangdese magmatic arc is interpreted to be initiated at a juvenile continental margin during the Late Triassic-Early Jurassic, although a possible intra-oceanic arc setting cannot be excluded.

1. Introduction

The Qinghai-Tibetan Plateau was built up due to the assemblage of a number of Gondwana-derived terranes during Mesozoic time, which was accompanied by closure of the Paleo- and Neo-Tethys oceans (Dewey et al., 1988; Kapp et al., 2007; Yin and Harrison, 2000; Zhu et al., 2009, 2012, 2013). The Neo-Tethys was formed between Gondwana to the south and Eurasia to the north during the Late Permian to the Tertiary (Pan and Fang, 2010; Sengör, 1979), and finally closed due to the collision between India and Eurasian continents.

The Gangdese magmatic arc located in the southern Lhasa block was referred to as southern Gangdese belt or southern Lhasa subterrane by Zhu et al. (2009, 2011). This belt mainly consists of intermediate-felsic intrusions and associated volcano-sedimentary rocks, and has long been considered to be related to northward subduction of the Neo-Tethys. The understanding of this magmatic belt is critical to unravel the evolutionary history of the Neo-Tethys. In past decades, whereas the majority of workers studied the nature of the India-Asia collision and Cenozoic magma processes (e.g. Aitchison et al., 2007; Mo et al., 2008; Rowley, 1996; Yin and Harrison, 2000), some paid attention to the pre-collision magmatic and tectonic evolution of the Gangdese belt. For example, recent studies based on the felsic intrusions in the southern Lhasa Terrane suggested that the initial northward subduction of the Neo-Tethys began during the Late Triassic-Early Jurassic (Chu et al., 2006; Guo et al., 2013; Ji et al., 2009; Qu et al., 2007; Tang et al., 2010; Wu et al., 2010; Yang et al., 2008; Zhang et al., 2007), whereas others proposed they formed in the Middle Jurassic to Cretaceous (Barley et al., 2003; Mo et al., 2005a,b; Schärer et al., 1984; Searle et al., 1999, 2007; Wen et al., 2008; Zhu et al., 2011, 2013). Recently,

* Corresponding author. Tel.: +86 20 85290282.
E-mail address: Jifengxu@gig.ac.cn (J.-F. Xu).

http://dx.doi.org/10.1016/j.lithos.2014.04.019
0024-4937/

Zhu et al. (2011) reported that these Late Triassic-Early Jurassic magmatic rocks were generated by southward subduction of Bangong-Nujiang Tethys between the Qiangtang Terrane in the north and the Lhasa Terrane in the south during the Permian to Early Cretaceous, so the age of these rocks cannot reflect initiation of the northward subduction of the Neo-Tethys (Zhu et al., 2013). Another argument is whether the Gangdese magmatic arc was produced at an Andean-type active continental margin in the south prior to the Indian collision (e.g., Aitchison et al., 2007; Guo et al., 2013; Mo et al., 2008; Rowley, 1996; Yin and Harrison, 2000) or in an intra-oceanic arc setting (Aitchison et al., 2000; Dai et al., 2013; McDermid et al., 2002).

The Bima Formation (of the Sangri Group) volcanic rocks are widely distributed in the southern Lhasa Terrane. This paper presents systematic geochronological and geochemical analysis of these volcanic rocks, to determine the age of the volcanic rocks, to reveal their tectonic environment and to understand the evolution of the Neo-Tethys and the Lhasa Terrane.

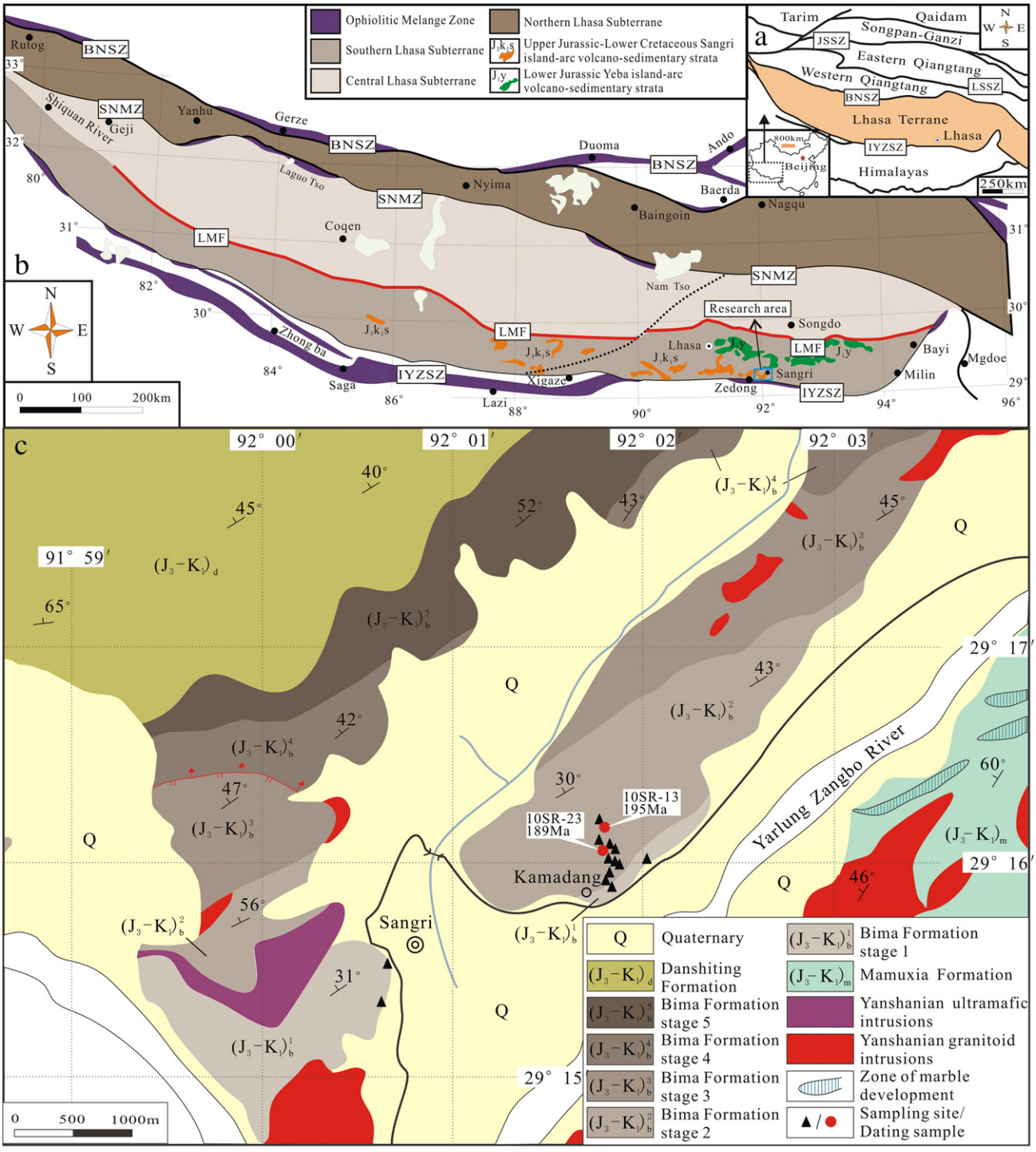

Fig. 1. (a) Tectonic outline of the Tibetan Plateau, (b) Tectonic framework of the Lhasa Terrane showing major tectonic subdivisions and distribution of Mesozoic volcanic rocks (after Sui et al., 2013), (c) Simplified geological map of the Sangri County region (after Kang et al., 2009). Abbreviations: JSSZ = Jinsha Suture Zone; LSSZ = Longmu Tso-Shuanghu Suture Zone; BNSZ = Bangong-Nujiang Suture Zone; SNMZ = Shiquan River-Nam Tso Mélange Zone; LMF = Luobadui-Milashan Fault; IYZSZ = Indus-Yarlung Zangbo Suture Zone.

2. Geological background and sampling

The Qinghai-Tibetan Plateau, from south to north, consists of the Himalaya, the Lhasa Terrane, the Western Qiangtang Terrane, the Eastern Qiangtang Terrane, and the Songpan-Ganzi flysch complex (Fig. 1a). These terranes are, respectively, separated by the Indus-Yarlung Zangbo (IYZSZ), Bangong-Nujiang (BNSZ), Longmu Tso-Shuanghu (LSSZ), and Jinsha (JSSZ) suture zones. Based on differences between basement rocks and sedimentary cover, the Lhasa Terrane is subdivided into the northern, central, and southern subterranes by the Shiquan River-Nam Tso Mélange Zone (SNMZ) and the Luobadui-Milashan Fault, respectively (LMF) (Fig. 1b) (Zhu et al., 2013). The southern part of the Lhasa Terrane is characterized by the widespread Gangdese magmatic arc of dominantly calc-alkaline granitoids that were emplaced from the Late Triassic (ca. 205 Ma) to the Early Tertiary (Chung et al., 2005; Guynn et al., 2006; Ji et al., 2009; Ma et al., 2013a,b; Wen et al., 2008; Zhu et al., 2011). The Mesozoic volcanic rocks in the southern Lhasa Terrane include the Lower Jurassic Yeba Formation that is distributed in the east of the Lhasa City (190-175 Ma) (Dong et al., 2006; Zhu et al., 2008), the Cretaceous adakite-like andesitic rocks of the Mamuxia Formation (136-93 Ma) of the Sangri Group (Kang et al., 2009, 2010; Zhu et al., 2009) (Fig. 1b), and the Cenozoic Linzizong Formation (Chen et al., 2010; He et al., 2007; Lee et al., 2007, 2012; Mo et al., 2003, 2007, 2008).

The Sangri Group consists of the Mamuxia and Bima formations, and is sporadically exposed in the central and eastern Gangdese magmatic arc in the southern Lhasa Terrane of the Sangri County in the east, and of the Saga County in the west. The exposed area extends over 800 km in length (Fig. 1b). The lower section of the Mamuxia Formation is mainly composed of andesite, locally interbedded with dacite and volcanic breccia, and an upper section of limestone breccia interbedded with dacite, capped by crystalline limestone. The total thickness is >2047 m, of which the volcanic rocks account for 43%. The Bima Formation comprises basalt, basaltic andesite, andesite and small amounts of dacite, interbedded with sandstone, slate and other sedimentary rocks (Figs. 1c and 2). The Bima Formation is divided into five lithological units, with a total thickness of 2200–2400 m, among which the thickness of volcanic sequence is about 1600–1800 m (Xia and Liu, 1997). Fossils and stratigraphic correlation indicate that the Sangri Group was deposited in a neritic to shallow marine or continental shelf environment (Zhu et al., 2003).

The studied samples were collected in the Kamadang region of the Sangri County, where the volcanic rocks of the Bima Formation are well exposed (Fig. 1c).

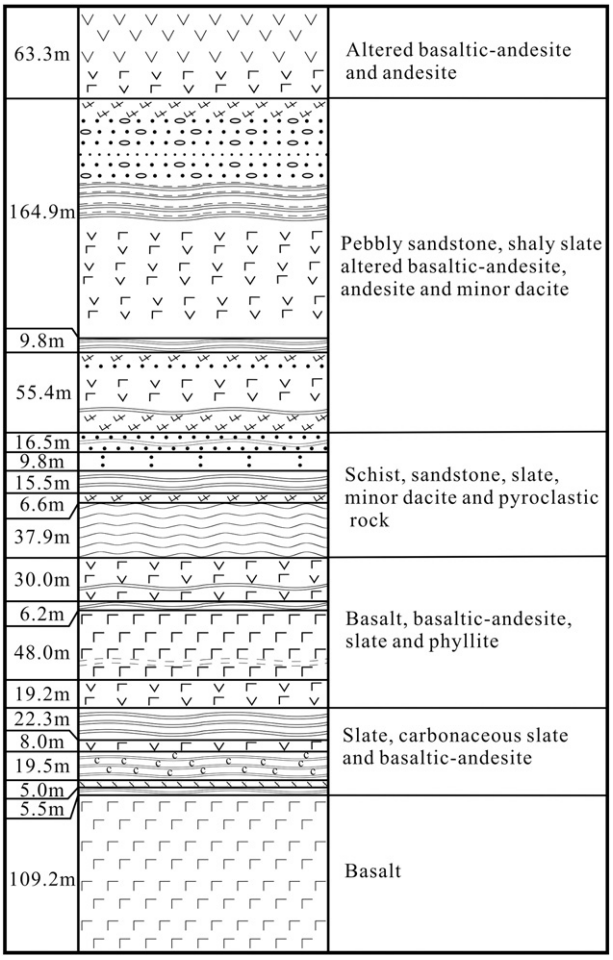

Fig. 2. Simplified stratigraphy of Bima Formation in northern area of Kamadang temple, Sangri County(the location is shown in Fig. 1c).

3. Analytical methods

3.1. LA-ICP-MS zircon U-Pb dating

Zircons were separated using conventional heavy liquid and magnetic separation techniques. All analyzed zircons were documented using both optical photomicrographs and Cathodoluminescence (CL) images (using a JEOL JXA-8100 Superprobe) prior to analysis at the State Key Laboratory of Isotope Geochemistry (SKLIG) at the Guangzhou Institute of Geochemistry, Chinese Academy of Sciences (GIGCAS), in order to characterize internal structures and choose potential target sites for U-Pb dating. LA-ICP-MS zircon U-Pb analyses were conducted on an Agilent 7500 ICP-MS equipped with a 193-nm laser which is housed at the State Key Laboratory of Geological Processes and Mineral Resources at the China University of Geosciences (Wuhan). Zircon 91500 was used as the standard to normalize isotopic fractionation during analysis of unknowns. The NIST610 glass was used as an external standard to calculate U, Th, and Pb concentrations of unknowns. Common Pb was corrected by ComPbCorr#3 151 (Anderson, 2002) for those with common ^{206}Pb > 1%. Further detailed descriptions of the instrumentation and analytical procedure for the LA-ICP-MS zircon U-Pb technique can be found in Liu et al. (2008, 2010). The $^{206}Pb/^{238}U$ ages are reported with analytical uncertainties at one-standard deviation (1σ) for each spot and two-standard deviation (2σ) for the weighted mean ages. The age calculations and concordia plots were made using Isoplot (version 3.0) (Ludwig, 2003).

3.2. Whole-rock geochemical analysis

After petrographic examination, the least-altered samples were selected for whole-rock geochemical analysis at the SKLIG, GIGCAS. Samples were firstly crushed to about 0.5 cm size and leached alternately by 5% HCL and HNO_3, then powdered to less than 200 mesh using a tungsten carbide ball mill and fluxed with $Li_2B_4O_7$ (1:9) at 1150–1200 °C to make homogeneous glass disks using an Analymate V8C automatic fusion machine. Major element oxides were analyzed using a Rigaku RIX 2000 X-ray fluorescence spectrometer with analytical precision ranging from 1% to 5% (Li et al., 2005).

Trace element compositions were analyzed using an inductively coupled plasma-mass spectrometer (Perkin-Elmer Sciex ELAN 6000 ICP-MS). Samples were first digested with a mixture of HF + HNO_3 in high-pressure Teflon bombs at 185 °C for two days. Pure single element Rh standard solutions were used for internal calibration, and standards GSR-1, GSR-2, GSR-3, W-2, SARM-4, MRG-1 and SY-4 were used as reference materials. The precision was higher than 5% for most elements, as indicated by multiple analyses of standards (Liu et al., 1996).

3.3. Whole-rock Sr-Nd isotope analysis

Samples for Sr and Nd isotopic analyses were dissolved in an acidic mixture of HF, HNO_3, and $HClO_4$ in Teflon bombs and separated by conventional cation-exchange techniques (Liang et al., 2003). Sr and Nd isotopic measurements were performed on a Triton thermal ionization mass spectrometer (TIMS) and Micromass Isoprobe multicollector ICP-MS (MC-ICP-MS), respectively, at the SKLIG, GIGCAS. Mass fractionation corrections for Sr and Nd isotopic ratios were based on $^{86}Sr/^{88}Sr = 0.1194$ and $^{146}Nd/^{144}Nd = 0.7219$, respectively. The $^{87}Sr/^{86}Sr$ ratio of the NBS 987 Sr standard was 0.710258 ± 7 (2σ), and the $^{143}Nd/^{144}Nd$ ratios of the La Jolla and JNDI-1 Nd standard solutions were 0.511841 ± 3 (2σ) and 0.512104 ± 5 (2σ), respectively.

4. Results

4.1. Zircon U-Pb age

Zircon U-Pb isotopic data of samples 10SR-13 and 10SR-23 are presented in Table 1. Zircon grains of sample 10SR-13 (andesite) are mostly prismatic and euhedral in shape (Fig. 3), and are 100–200 μm in length, with length-to-width ratios of 2:1–3:1. Magmatic oscillatory zonation is shown in some grains in the CL image, although it is not always clear (Fig. 3). Uranium and Th contents of analyzed zircons are 78–218 ppm and 50–223 ppm, respectively, with Th/U ratios ranging from 0.52–1.02, implying an origin of magmatic crystallization (Belousova et al., 2002; Wu and Zheng, 2004). Seventeen analyses were performed on 17 zircon grains, yielding concordant $^{206}Pb/^{238}U$ ages ranging from 186 to 204 Ma, with a weighted mean age of 195 ± 3 Ma (MSWD = 1.6) (Fig. 4a).

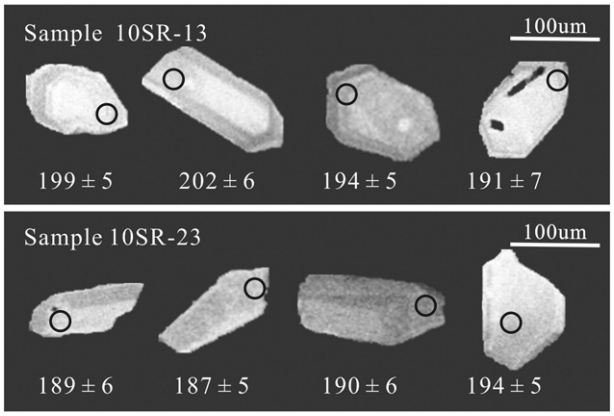

Fig. 3. CL images of representative zircon grains from samples 10SR-13 and 10SR-23, showing internal structures, analytical locations, and apparent $^{206}Pb/^{238}U$ ages.

Zircon grains from sample 10SR-23 (Volcanic tuff) are mostly prismatic and subhedral in shape (Fig. 3), and are 100–140 μm in length, with length-to-width ratios of 2:1–3:1. They show no obvious

Table 1
Zircon LA-ICP-MS U-Pb analyzing results for sample 10SR-13 and 10SR-23.

spot	Pb	Th	U	Th/U	Common-Pb corrected isotopic ratios (±1σ)						Common-Pb corrected isotopic ages (±1σ)						Concordance
	ppm	ppm	ppm		$^{207}Pb^*/^{206}Pb^*$		$^{207}Pb^*/^{235}U$		$^{206}Pb^*/^{238}U$		$^{207}Pb/^{206}Pb$		$^{207}Pb/^{235}U$		$^{206}Pb/^{238}U$		
Sample: 10SR-13																	
10SR-13-01	4.67	105	112	0.94	0.04995	0.00726	0.19823	0.03035	0.02926	0.00076	191	307	184	26	186	5	98%
10SR-13-02	5.28	72	127	0.56	0.05694	0.00711	0.24158	0.02905	0.03170	0.00089	500	278	220	24	201	5	91%
10SR-13-03	5.29	104	124	0.84	0.05022	0.00684	0.21080	0.02740	0.03129	0.00085	206	289	194	23	199	5	97%
10SR-13-04	4.72	76	123	0.62	0.05203	0.00750	0.20660	0.02712	0.02975	0.00084	287	300	191	23	189	5	99%
10SR-13-05	8.72	147	211	0.70	0.04677	0.00517	0.20041	0.02017	0.03145	0.00065	39	244	185	17	200	4	92%
10SR-13-06	3.28	51	79	0.64	0.05187	0.00954	0.22867	0.04400	0.03115	0.00127	280	374	209	36	198	8	94%
10SR-13-07	9.21	223	218	1.02	0.05200	0.00573	0.20783	0.02121	0.02928	0.00062	287	254	192	18	186	4	96%
10SR-13-08	6.70	122	165	0.73	0.05144	0.00601	0.21114	0.02289	0.02988	0.00071	261	248	194	19	190	4	97%
10SR-13-09	5.81	104	148	0.70	0.04930	0.00626	0.21624	0.02857	0.03047	0.00074	161	274	199	24	193	5	97%
10SR-13-10	4.98	82	124	0.66	0.05128	0.00713	0.22476	0.02925	0.03176	0.00101	254	293	206	24	202	6	97%
10SR-13-11	5.52	99	140	0.71	0.05566	0.00702	0.23792	0.02817	0.03159	0.00077	439	283	217	23	200	5	92%
10SR-13-12	4.89	77	135	0.57	0.05083	0.00712	0.21330	0.02873	0.03054	0.00108	232	296	196	24	194	7	98%
10SR-13-13	4.12	68	111	0.61	0.04984	0.00741	0.20812	0.02968	0.03050	0.00088	187	315	192	25	194	5	99%
10SR-13-14	5.78	80	155	0.52	0.05194	0.00468	0.21891	0.01946	0.03099	0.00079	283	207	201	16	197	5	97%
10SR-13-15	5.15	101	126	0.80	0.05138	0.00761	0.22909	0.03277	0.03289	0.00123	257	311	209	27	209	8	99%
10SR-13-16	2.92	50	78	0.64	0.04932	0.00864	0.20945	0.03901	0.03011	0.00111	165	363	193	33	191	7	99%
10SR-13-17	8.18	193	191	1.02	0.05318	0.00448	0.23016	0.01772	0.03219	0.00073	344	193	210	15	204	5	97%
Sample: 10SR-23																	
10SR-23-01	8.60	156	225	0.69	0.05513	0.00536	0.23281	0.02201	0.03054	0.00064	417	218	212	18	194	4	90%
10SR-23-02	4.69	68	123	0.55	0.04957	0.00575	0.20750	0.02270	0.03052	0.00083	176	257	191	19	194	5	98%
10SR-23-03	5.06	76	138	0.55	0.05488	0.00569	0.21412	0.01981	0.02977	0.00103	406	233	197	17	189	6	95%
10SR-23-04	5.50	72	156	0.46	0.04854	0.00597	0.19688	0.02337	0.02926	0.00080	124	267	182	20	186	5	98%
10SR-23-05	4.51	54	132	0.41	0.05040	0.00742	0.20194	0.02893	0.03010	0.00075	213	311	187	24	191	5	97%
10SR-23-06	4.44	49	126	0.39	0.04927	0.00675	0.20844	0.02942	0.03034	0.00103	161	293	192	25	193	6	99%
10SR-23-07	2.96	40	81	0.50	0.05180	0.00763	0.20534	0.02930	0.03000	0.00097	276	307	190	25	190	6	99%
10SR-23-08	5.30	62	151	0.41	0.05002	0.00763	0.19746	0.02902	0.02972	0.00097	194	322	183	25	189	6	96%
10SR-23-09	4.31	61	120	0.50	0.05023	0.00728	0.20622	0.03353	0.02949	0.00087	206	304	190	28	187	5	98%
10SR-23-10	7.68	106	206	0.51	0.05038	0.00429	0.20693	0.01797	0.03009	0.00071	213	-1	191	15	191	4	99%
10SR-23-11	2.54	32	73	0.44	0.05263	0.00878	0.20576	0.03223	0.02979	0.00093	322	331	190	27	189	6	99%
10SR-23-12	4.82	76	128	0.59	0.04999	0.00601	0.20384	0.02517	0.02983	0.00088	194	259	188	21	189	5	99%
10SR-23-13	3.29	34	90	0.38	0.05594	0.00679	0.23012	0.02861	0.03010	0.00089	450	272	210	24	191	6	90%
10SR-23-14	5.77	85	153	0.56	0.05392	0.00602	0.22132	0.02385	0.03032	0.00086	369	258	203	20	192	5	94%
10SR-23-15	4.64	54	137	0.40	0.05001	0.00796	0.18942	0.02859	0.02815	0.00083	194	333	176	24	179	5	98%
10SR-23-16	4.39	62	116	0.53	0.05248	0.00763	0.21418	0.02892	0.03014	0.00088	306	304	197	24	191	5	97%
10SR-23-17	5.69	84	152	0.55	0.05127	0.00654	0.19742	0.02384	0.02823	0.00087	254	270	183	20	179	5	98%
10SR-23-18	5.37	68	149	0.46	0.05617	0.00598	0.21731	0.02206	0.02852	0.00089	457	234	200	18	181	6	90%

Pb* = corrected for ^{204}Pb using the program of Anderson (2002).

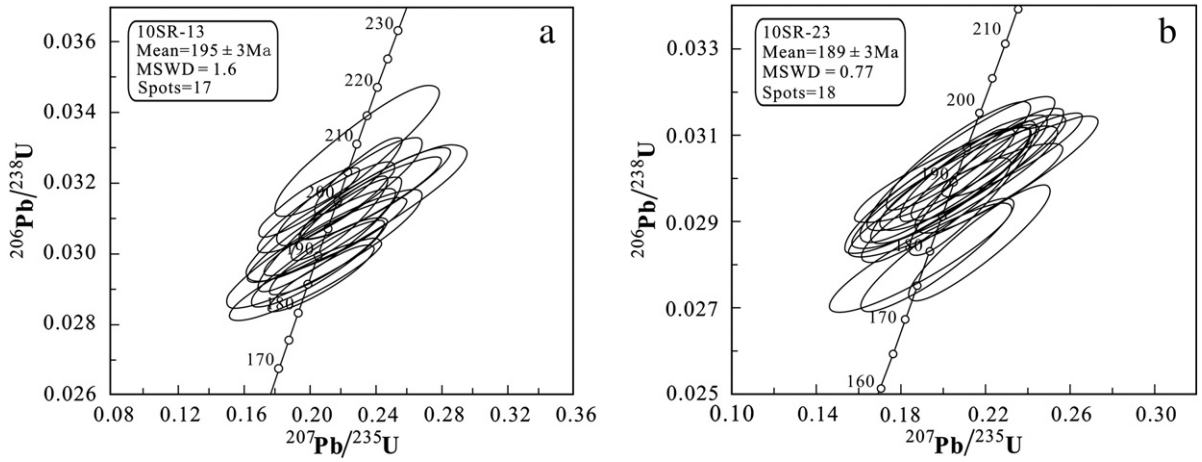

Fig. 4. Zircon U-Pb concordia diagrams of Bima Formation volcanic rocks.

Table 2
Whole-rock geochemical data for the volcanic rocks of the Bima Formation.

10SR-23		10SR-27	10SR-32	10SR-39	10SR-24	10SR-28	10SR-31	10SR-33	10SR-35	10SR-41	10SR-43	10SR-48	10SR-13	10SR-44	10SR-08
Volcanic tuff		Basalt I			Basalt II							Andesite			Dacite
XRF major elements (wt.%)															
SiO_2	48.81	49.19	50.03	50.09	51.84	47.08	49.22	49.48	49.30	54.09	52.38	56.90	60.74	55.29	67.04
TiO_2	1.55	1.28	1.16	0.83	0.92	1.05	1.27	1.02	0.91	0.69	0.91	0.99	0.86	0.40	0.52
Al_2O_3	32.53	17.12	16.02	17.27	19.70	19.60	20.37	19.87	20.74	17.37	19.72	16.39	20.68	16.75	18.18
TFe_2O_3	8.10	11.47	11.18	10.59	10.04	14.22	10.57	11.58	12.44	9.23	9.76	7.75	5.90	11.33	3.64
MnO	0.05	0.16	0.16	0.16	0.24	0.74	0.22	0.22	0.14	0.17	0.15	0.08	0.08	0.11	0.15
MgO	0.78	8.02	7.33	7.25	4.48	2.74	5.44	4.63	4.01	4.67	5.51	3.99	1.33	3.92	1.27
CaO	0.18	7.65	9.73	8.08	5.36	12.26	4.18	4.75	4.83	7.49	3.30	2.92	2.53	3.45	3.45
Na_2O	2.24	1.67	2.68	3.47	4.99	0.65	5.21	5.30	4.76	2.55	4.73	4.19	4.25	0.88	2.47
K_2O	1.61	0.08	0.06	0.21	0.41	0.16	0.39	0.22	0.77	0.63	0.24	2.03	1.36	1.24	1.32
P_2O_5	0.05	0.17	0.15	0.14	0.16	0.14	0.31	0.25	0.07	0.17	0.16	0.35	0.10	0.14	0.13
LOI	4.08	3.05	1.30	1.72	1.69	1.16	2.68	2.51	1.85	2.83	3.03	4.45	2.07	6.80	1.75
TOTAL	99.99	99.87	99.80	99.82	99.82	99.79	99.86	99.85	99.82	99.89	99.89	100.04	99.90	100.31	99.91
Mg#	18.4	62.0	60.5	61.5	51.0	31.0	54.5	48.3	42.9	54.1	56.8	54.5	34.4	44.6	44.8
ICP-MS trace elements (ppm)															
Sc	35.8	28.6	25.9	38.0	29.6	39.3	38.5	34.0	25.9	27.1	21.6	13.9	20.8	8.9	14.6
V	164	211	191	279	297	318	274	284	214	251	278	170	169	85.6	70.7
Cr	59	268	236	402	33	161	18	27	51	78	25	82	83	66	113
Co	8	47	48	43	26	26	31	30	33	27	30	21	12	15	5
Ni	19	174	157	132	7	47	8	8	32	16	9	42	12	22	7
Rb	36	2	1	3	10	2	12	5	20	11	6	73	27	28	21
Sr	500	278	435	741	364	275	550	578	848	500	614	329	342	245	296
Y	52.4	20.0	18.3	18.0	19.6	31.1	24.7	23.2	15.9	18.4	13.8	17.1	16.0	9.87	26.3
Zr	317	81	72	71	66	99	81	69	84	42	65	211	98	69	121
Nb	10.3	3.60	3.06	1.74	2.28	3.10	3.09	2.60	3.26	0.93	1.32	8.37	3.66	2.05	4.33
Cs	5.17	0.88	0.15	0.54	5.23	0.81	1.65	1.15	3.18	1.42	1.60	12.6	3.30	4.35	1.90
Ba	293	33.4	36.4	101	140	49.0	229	122	250	138	80.1	158	220	252	224
La	43.4	6.04	5.88	6.98	12.5	17.6	12.2	12.3	11.3	5.30	7.34	29.8	12.2	11.5	20.9
Ce	95.6	15.1	14.0	16.7	28.0	38.4	31.0	28.6	25.6	12.8	17.9	61.4	26.1	23.1	44.7
Pr	12.4	2.26	2.11	2.35	3.88	5.32	4.63	4.12	3.48	1.98	2.63	7.61	3.46	2.74	5.69
Nd	52.3	10.8	9.87	11.1	16.8	22.9	21.1	19.1	15.6	9.38	12.3	29.5	13.9	11.7	22.1
Sm	11.2	3.14	2.78	2.92	3.74	5.14	5.09	4.64	3.78	2.58	3.10	5.27	3.13	2.23	4.27
Eu	2.70	0.92	0.96	1.03	1.20	1.36	1.49	1.39	1.36	0.86	0.77	1.18	1.09	0.56	1.08
Gd	10.1	3.62	3.41	3.19	3.68	5.36	4.94	4.61	3.69	2.92	3.11	4.42	2.88	2.00	4.17
Tb	1.70	0.60	0.57	0.52	0.55	0.89	0.77	0.71	0.56	0.50	0.49	0.63	0.47	0.30	0.71
Dy	10.4	3.87	3.55	3.29	3.32	5.36	4.68	4.29	3.37	3.20	2.86	3.41	2.87	1.78	4.61
Ho	2.24	0.81	0.75	0.71	0.75	1.17	1.02	0.92	0.70	0.71	0.59	0.69	0.58	0.38	0.99
Er	6.24	2.11	2.02	1.93	2.16	3.19	2.69	2.51	1.89	2.02	1.58	1.88	1.63	1.15	2.84
Tm	0.98	0.31	0.30	0.28	0.31	0.49	0.41	0.36	0.28	0.31	0.23	0.28	0.25	0.19	0.45
Yb	6.70	2.00	1.90	1.89	2.12	3.17	2.58	2.35	1.92	2.05	1.49	1.86	1.62	1.44	2.93
Lu	1.03	0.31	0.29	0.28	0.34	0.51	0.41	0.38	0.31	0.33	0.23	0.28	0.27	0.23	0.47
Hf	8.97	1.93	1.83	1.73	1.67	2.44	2.14	1.69	2.07	1.20	1.70	5.55	2.54	2.11	3.45
Ta	0.74	0.24	0.21	0.11	0.14	0.20	0.18	0.15	0.18	0.05	0.08	0.62	0.24	0.16	0.35
Pb	11.1	2.91	11.2	3.46	8.52	12.8	10.8	7.23	4.10	4.11	3.22	24.2	12.2	4.57	14.6
Th	8.31	0.84	0.79	0.76	1.48	2.01	1.97	1.64	0.69	0.57	0.83	13.2	2.14	1.56	4.15
U	2.26	0.26	0.25	0.23	0.45	0.56	0.50	0.44	0.17	0.21	0.36	3.63	0.61	0.85	1.16
Eu*	0.78	0.83	0.95	1.04	0.99	0.79	0.91	0.92	1.11	0.95	0.76	0.75	1.11	0.81	0.79

LOI = loss on ignition. Mg# = $100 \times Mg^{2+}/(Mg^{2+}+TFe^{2+})$, TFeO* = $0.8998 \times TFe_2O_3$. Eu* = $Eu/0.058/(Sm/0.153 \times Gd/0.2055)^{1/2}$.

oscillatory zonation, similar to typical internal features of zircons from mafic magmas (Sui et al., 2013). They also have relatively uniform concentrations of U (73-225 ppm), Th (32–156 ppm), with Th/U of 0.38–0.69, which are lower than those of sample 10SR-13. These zircons are also interpreted to be of magmatic origin. Eighteen analyses performed on 18 zircon grains yielded concordant $^{206}Pb/^{238}U$ ages of 179 to 194 Ma and a weighted mean age of 189 ± 3 Ma (MSWD = 0.77) (Fig. 4b).

4.2. Geochemical data

Geochemical compositions of the Bima Formation volcanic rocks are listed in Table 2. On the Zr/TiO_2 vs. Nb/Y diagram (Fig. 5a) of Winchester and Floyd (1976), the samples are mainly plotted in the subalkaline basalt, andesite/basalt and andesite fields, excepting one dacite sample. All basalts are tholeiitic, whereas andesites include both tholeiitic and calc-alkaline (Fig.5b). Sample 10SR-23 plots on the andesite field, but it shows abnormal geochemical characteristics, such as the extremely low contents of SiO_2 (48.81 wt%), MgO (0.78 wt%), CaO (0.18 wt%), Mg # (18.4), and unusually high contents of Al_2O_3 (32.53 wt%). The sample contains a large amount of chloritoid, showing that it has experienced low-grade metamorphism, so the following discussion doesn't concern this sample.

4.2.1. Basalts

Based on geochemical characteristics, the Bima Formation basalts are divided into two groups. Basalts of Group I have relatively high contents of MgO (7.25–8.02 wt%), Mg# (60.5–62.0), Cr (236–402 ppm), and Ni (132–174 ppm), and low contents of Al_2O_3 (16.02–17.27 wt%), implying relatively primitive magma compositions (Leat et al., 2002). Basalts of Group II have lower but a wider range of MgO (2.74–5.51 wt%), Mg# (31.0–56.8), Cr (27–161 ppm), and Ni (7–47 ppm), and higher Al_2O_3 (17.37–20.74 wt%) than those of Group I, showing characteristics of more evolved magmas.

Basalts in both groups have similar rare earth element (REE) distribution patterns (Fig. 6a), although basalts in Group II have higher total REE than Group I (average of 77.6 ppm and 51.2 ppm, respectively). They show light LREE enrichment, with the $(La/Yb)_N$ ratio slightly different between groups, with an average value of 2.35 in Group I and 3.57 in Group II. Average Eu* values of Groups I and II are 0.94 and 0.92, respectively, showing no clear Eu anomalies. Primitive mantle normalized multi-element patterns of both groups exhibit enrichment in Sr and La, and depletion in high field strength elements (HFSEs) with Nb, Ta, and Ti negative anomalies, indicating typical characteristics of arc magmas (Fig. 6b).

4.2.2. Andesites and dacite

Three andesite samples from the Bima Formation show variable contents of SiO_2 (55.29–60.74 wt%), MgO (1.33–3.99 wt%), $Mg^{\#}$ (34.4–54.5), Cr (66–83 ppm), and Ni (12–42 ppm). Their REE distribution patterns (Fig. 6c) also show LREE enrichment. They have high $(La/Yb)_N$ (average of 7.54) and ΣREE (average of 90.1 ppm) and negative Eu anomalies (with an average Eu* of 0.89). Their primitive mantle-normalized multi-element patterns (Fig. 6d) exhibit characteristics of arc volcanic rocks (with enriched large ion lithophile elements and negative anomalies of Nb, Ta, and Ti). The dacite sample (SiO_2 = 67.04 wt%) has high Al_2O_3 (18.18 wt%) and low MgO (1.27 wt%), CaO (3.45 wt%) and TiO_2 (0.52 wt%) contents. The REE and primitive mantle-normalized multi-element patterns is similar to the andesites, with enrichment of LREE and minor negative Eu anomalies (0.79).

4.3. Sr-Nd isotopic analysis

Eleven Bima Formation samples were collected from the southern Lhasa Terrane in the Sangri County and analyzed for whole-rock Sr-Nd isotopic compositions. The results are shown in Table 3. Generally, basalts in Group I have higher positive $\varepsilon_{Nd}(t)$ values (+6.90 to +7.02) and lower initial $^{87}Sr/^{86}Sr$ ratios (0.7040-0.7041) than those of Group II (with $\varepsilon_{Nd}(t)$ = +4.58 to +6.86 and initial $^{87}Sr/^{86}Sr$ = 0.7040-0.7050). The andesite samples show lower $\varepsilon_{Nd}(t)$ values (+4.09 to +4.46) and variable initial $^{87}Sr/^{86}Sr$ ratios (0.7032–0.7048). The dacite sample have lowest $\varepsilon_{Nd}(t)$ (+3.19) values and highest initial $^{87}Sr/^{86}Sr$ ratio (0.7055) (Fig. 7).

5. Discussion

5.1. Petrogenesis

5.1.1. The Bima Formation basalt

Basalts of Group I have relatively high contents of MgO, Mg#, Cr and Ni, similar to high-Mg basalts (Bacon et al., 1997; Morra et al., 1997), demonstrating primitive magmatic features (Frey et al., 1978; Hess, 1992) without significant fractional crystallization of mafic minerals. Basalts of Group II, however, have considerably lower contents and larger variations of MgO, Mg#, Cr and Ni, suggesting that they have undergone fractional crystallization of mafic minerals during magmatic evolution (Perfit et al., 1980). The MgO vs. SiO_2 and CaO vs. SiO_2 diagrams (Fig. 8a, b) also support this conclusion. In addition, their high Al_2O_3 contents, positive Sr anomalies (Fig. 6b), and the lack of negative Eu anomalies (Fig. 6a) indicate that there was no fractional crystallization of plagioclase. In the $\varepsilon_{Nd}(t)$ vs. MgO and initial $^{87}Sr/^{86}Sr$ vs. MgO diagrams (Fig. 8c, d), samples show a crustal contamination trend.

In the $(Hf/Sm)_N$ vs. $(Ta/La)_N$ diagram (Fig. 9a), most of the basalts plot in the field of hydrated mantle source, among which two of them plot in the transition zone between DM and hydrated mantle source, showing that their source region was affected by subduction-related fluids (La Fléche et al., 1998). Generally any melts or fluids sourced

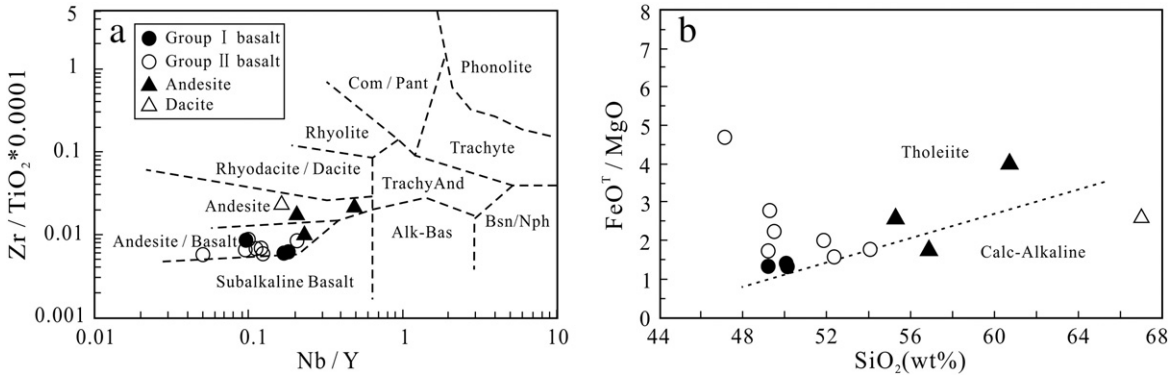

Fig. 5. (a) $Zr/TiO_2 \times 0.0001$ vs. Nb/Y diagram (Winchester and Floyd, 1976); (b) FeOT/MgO vs. SiO_2 diagram (Miyashiro, 1974).

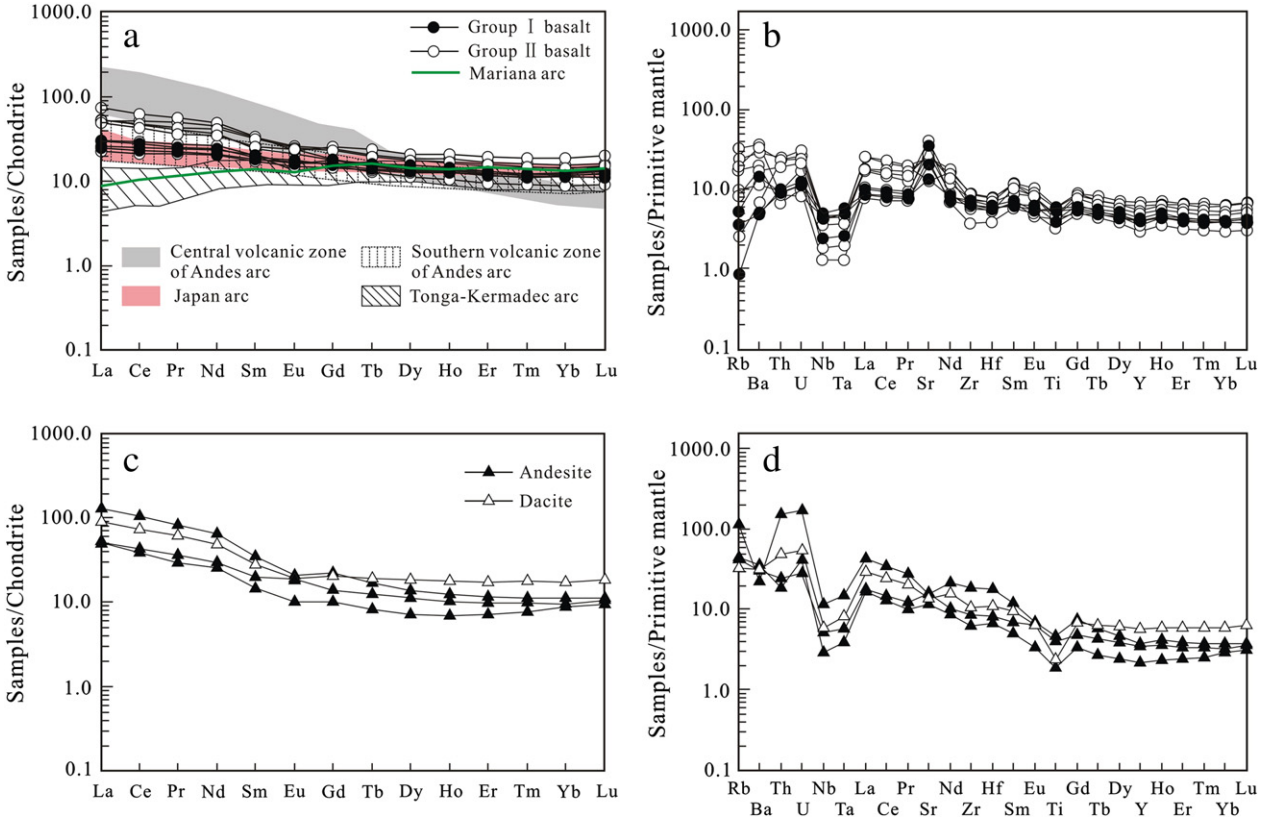

Fig. 6. Chondrite-normalized REE and primitive-mantle-normalized trace element patterns for Bima Formation volcanic rocks, (a) and (b) are basalts, (c) and (d) are andesites and dacite. (Data of Central and Southern volcanic zone of Andes arc is from Winter, 2010; data of Tonga-Kermadec arc is from Smith et al., 2010; data of Japan arc is from Takahashi et al., 2013; and dada of Mariana arc is from Peate and Pearce, 1998; Chondrite-normalizing and primitive-mantle normalizing values are from Sun and McDonough, 1989).

from subducted sediments change isotopic compositions of the mantle source region. The Bima Formation basalts have positive $\varepsilon_{Nd}(t)$ values (+4.58 to +7.02)and low initial $^{87}Sr/^{86}Sr$ values (0.7040–0.7050). On the $\varepsilon_{Nd}(t)$ vs. initial $^{87}Sr/^{86}Sr$ diagram (Fig. 7), samples are plotted in or near the Neo-Tethyan ophiolite. The low ratios of Th/Ce (0.03–0.09), Th/Nb (0.21–0.81), and Nb/Zr (0.02–0.04) are different from island arc basalts affected by subducted sediments (Gertisser and Keller, 2003; Kimura and Yoshida, 2006; Peng et al., 2008; Petrone et al., 2003; Seghedi et al., 2001; Sui et al., 2013). On the Ba/Th vs. initial $^{87}Sr/^{86}$ Sr diagram (Fig. 9b), basalts are plotted near the Indian MORB, demonstrating a trend of being affected by subducted slab-derived fluids other than subducted sediments.

Geochemical results demonstrate that magmas of the Bima Formation volcanic rocks were most likely generated by partial melting of a MORB-like depleted mantle wedge that was metasomatized by subduction-related fluids or melts (Gertisser and Keller, 2003; Plank and Langmuir, 1998). The original magmas subsequently experienced crustal contamination and fractional crystallization during their ascent.

5.1.2. The Bima Formation andesite and dacite

Two general models have been proposed to address the generation of intermediate-silicic magmas in subduction zones: (1) Extensive fractional crystallization of mantle-derived basaltic melts, coupled with crustal contamination (e.g., Bacon and Druitt, 1988; Bonin, 2004; Pin and Paquette, 1997); and (2) crustal anatexis caused by mantle-derived mafic magmas with distinct isotopic compositions (Guffanti et al., 1996; Roberts and Clemens, 1993; Tepper et al., 1993; Zhu et al., 2007, 2012). The Bima Formation andesites have the following characteristics: (1) The Bima Formation volcanic rocks mainly include basalt and andesite, including only one dacite sample. This is relevant to the first model (Riley et al., 2001; Yalew and Yirgu, 2003), and different from the second model (Chen et al., 2013; Guffanti et al., 1996;

Table 3
Sr and Nd isotope data for the volcanic rocks of the Bima Formation.

Sample	Group	Sm	Nd	Rb	Sr	$^{87}Rb/^{86}Sr$	$^{87}Sr/^{86}Sr \pm 2\sigma$	$(^{87}Sr/^{86}Sr)_i$	$^{147}Sm/^{144}Nd$	$^{143}Nd/^{144}Nd \pm 2\sigma$	$(^{143}Nd/^{144}Nd)_i$	T_{DM}(Ga)	$\varepsilon_{Nd}(t)$
10SR-08	Dacite	4.27	22.1	20.8	296	0.2035	0.706039 ± 4	0.705489	0.1168	0.512702 ± 7	0.512557	0.708	3.19
10SR-13	Andesite	3.13	13.9	26.8	342	0.2270	0.705403 ± 6	0.704789	0.1358	0.512791 ± 10	0.512622	0.706	4.46
10SR-48		5.27	29.5	72.6	329	0.6383	0.704906 ± 4	0.703182	0.1078	0.512876 ± 6	0.512603	0.597	4.09
10SR-27	Group	3.14	10.8	2.31	278	0.0240	0.704191 ± 6	0.704126	0.1768	0.512967 ± 8	0.512747	0.762	6.90
10SR-32	I Basalt	2.78	9.87	0.55	435	0.0037	0.704110 ± 5	0.704100	0.1704	0.512965 ± 9	0.512753	0.656	7.02
10SR-39		2.92	11.1	3.35	741	0.0131	0.704020 ± 6	0.703984	0.1586	0.512945 ± 9	0.512748	0.572	6.92
10SR-28	Group	5.14	22.9	1.65	275	0.0174	0.705074 ± 6	0.705027	0.1356	0.512836 ± 6	0.512667	0.616	5.35
10SR-33	IIBasalt	4.64	19.1	5.29	578	0.0264	0.704609 ± 5	0.704538	0.1469	0.512811 ± 7	0.512628	0.778	4.58
10SR-41		2.58	9.38	11.0	500	0.0634	0.704150 ± 6	0.703979	0.1665	0.512876 ± 10	0.512669	0.890	5.38
10SR-43		3.10	12.3	6.29	614	0.0296	0.704164 ± 4	0.704084	0.1530	0.512876 ± 8	0.512745	0.544	6.86
10SR-23	Volcanic tuff	11.2	52.3	35.9	500	0.2078	0.705515 ± 5	0.704954	0.1291	0.512860 ± 8	0.512699	0.526	5.97

$\varepsilon_{Nd}(t) = [(^{143}Nd/^{144}Nd)s/(^{143}Nd/^{144}Nd)_{CHUR} - 1] \times 10{,}000$, $T_{DM} = \ln[(^{143}Nd/^{144}Nd)s - (^{143}Nd/^{144}Nd)_{DM}]/[(^{143}Sm/^{144}Nd)s - (^{147}Sm/^{144}Nd)_{DM}]/\lambda$ (DePaolo, 1988).
In the calculation $(^{143}Nd/^{144}Nd)_{CHUR} = 0.512638$, $(^{147}Sm/^{144}Nd)_{CHUR} = 0.1967$, $(^{143}Nd/^{144}Nd)_{DM} = 0.51315$, $(^{147}Sm/^{144}Nd)_{DM} = 0.2136$ and t = 190.0 Ma.

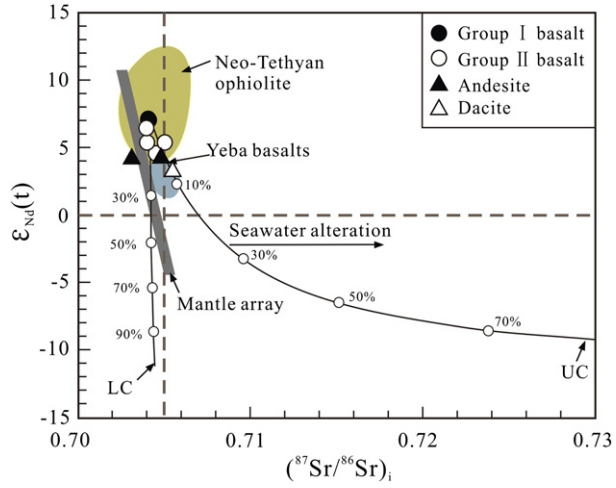

Fig. 7. $\varepsilon_{Nd}(t)$ vs. $(^{87}Sr/^{86}Sr)_i$ diagram for Bima Formation volcanic rocks (Data of Neo-Tethyan opholite are from Mahoney et al., 1998; Xu and Castillo, 2004; Zhang et al., 2005; data of the Yeba basalts is from Zhu et al., 2008; and data for the upper and lower crust are from Ma et al., 2013a and Wen et al., 2008).

Roberts and Clemens, 1993; Tepper et al., 1993; Zhu et al., 2007, 2008, 2012); (2) Although the andesites and dacite have different initial $^{87}Sr/^{86}Sr$ ratios and $\varepsilon_{Nd}(t)$ values with the basalts, but this can also be reached by 10% assimilation of upper curst (Fig. 7). In addition, the $\varepsilon_{Nd}(t)$ vs. MgO and initial $^{87}Sr/^{86}Sr$ vs. MgO diagrams show linear relationships with the basalts, showing crust assimilation trend (Fig. 8c, d); (3) In the MgO vs. SiO_2 and CaO vs. SiO_2 diagrams (Fig. 8a, b), the andesites and dacite also show a linear relationship with the basalts, suggesting fractional crystallization of mafic minerals.

In summary, we suggest that the Bima Formation andesites and dacite were likely derived from the same source as the basalts, but the original magmas experienced AFC processes to generate the evolved magmas.

5.2. Tectonic setting

According to petrographic observations and LOI (Table 2), the Bima Formation volcanic rocks have generally undergone alteration and low-grade metamorphism at greenschist facies, so any further discussion must take into account the influence of these events. Generally, it is considered that the transition elements (such as Cr, Ni), REEs, and HFSEs, as well as Th and Ti in mafic rocks, are relatively stable during alteration and low-grade metamorphism (Bienvenu et al., 1990; Staudigel et al., 1996). The following discussion assumes the same is true for the Bima Formation mafic volcanics.

Contents of Zr, V, Ti, and Y contained in basalt can be effectively used to distinguish between island-arc basalt and non-island-arc basalt (e.g., Pearce and Cann, 1973; Pearce and Norry, 1979). Basalts of Group I have Ti/V ratios of 17.83–36.40 which are similar to those of the basalts (16.48–27.78) of Group II, they are plotted in the MORB to island arc tholeiitic basalt fields in the V vs. Ti diagram (Shervais, 1982)

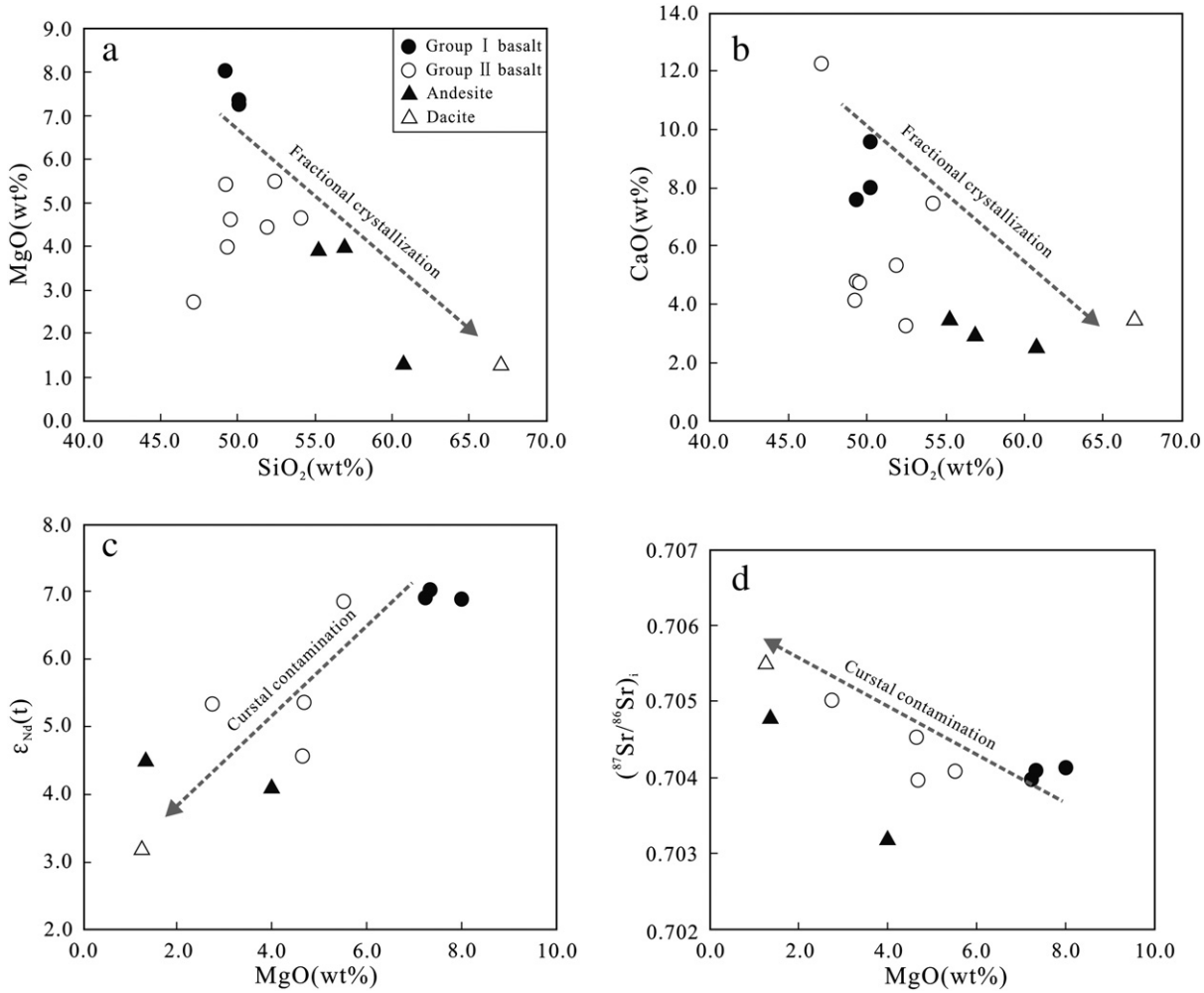

Fig. 8. Chemical variation diagrams for Bima Formation volcanic rocks. (a) MgO vs. SiO_2, (b) CaO vs. SiO_2, (c) $\varepsilon_{Nd}(t)$ vs. MgO, (d) $(^{87}Sr/^{86}Sr)_i$ vs MgO.

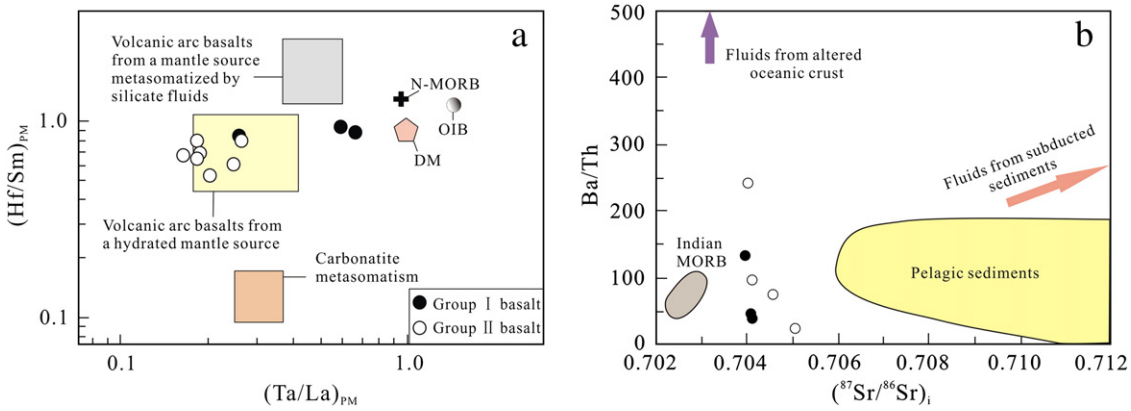

Fig. 9. (a) $(Hf/Sm)_N$ vs. $(Ta/La)_N$ discrimination diagram for Bima Formation basalts (after La Flèche et al., 1998), where N denotes normalized to the primitive mantle values of Sun and McDonough (1989). (b) Ba/Th vs. $^{87}Sr/^{86}Sr(i)$ discrimination diagram for Bima Formation basalts. The data for fluids released from a subducted slab are from Tatsumi and Kogiso (1997) and Ayers (1998) and those of global sediments are from Ben Othman et al. (1989), Vroon et al. (1993, 1995), and Stolz et al. (1988, 1990).

(Fig. 10a). The Zr content (42–99 ppm) is low and the rocks fall in the fields of island arc basalts and MORB in the Ti vs. Zr diagram (Fig. 10b). In Th/Yb vs. Ta/Yb and Th/Hf vs. Ta/Hf diagrams (Fig. 10c, d), the basalts mostly plot in the active continental margin and intra-oceanic arc basalt fields. The basalts also show typical island arc basalt characteristics (such as depletion in Nb, Ta, Ti, Zr, and Hf), suggesting that they were generated in a subduction environment. Combination with the results of Early Jurassic granitic plutons recently reported in the southern Lhasa Terrane (Chu et al., 2006; Guo et al., 2013; Ji et al., 2009; Qu et al., 2007; Tang et al., 2010; Yang et al., 2008; Zhang et al., 2007), we consider that the southern Lhasa Terrane underwent northward subduction of the Neo-Tethys during Early Jurassic times.

The remaining question is whether the Bima Formation volcanic rocks were developed at a continental margin or on intra-oceanic arc basement. The basalts are tholeiitic with low contents of K_2O and Th, low $(La/Yb)_N$ and initial $^{87}Sr/^{86}Sr$ ratios, and depleted in Nd, showing

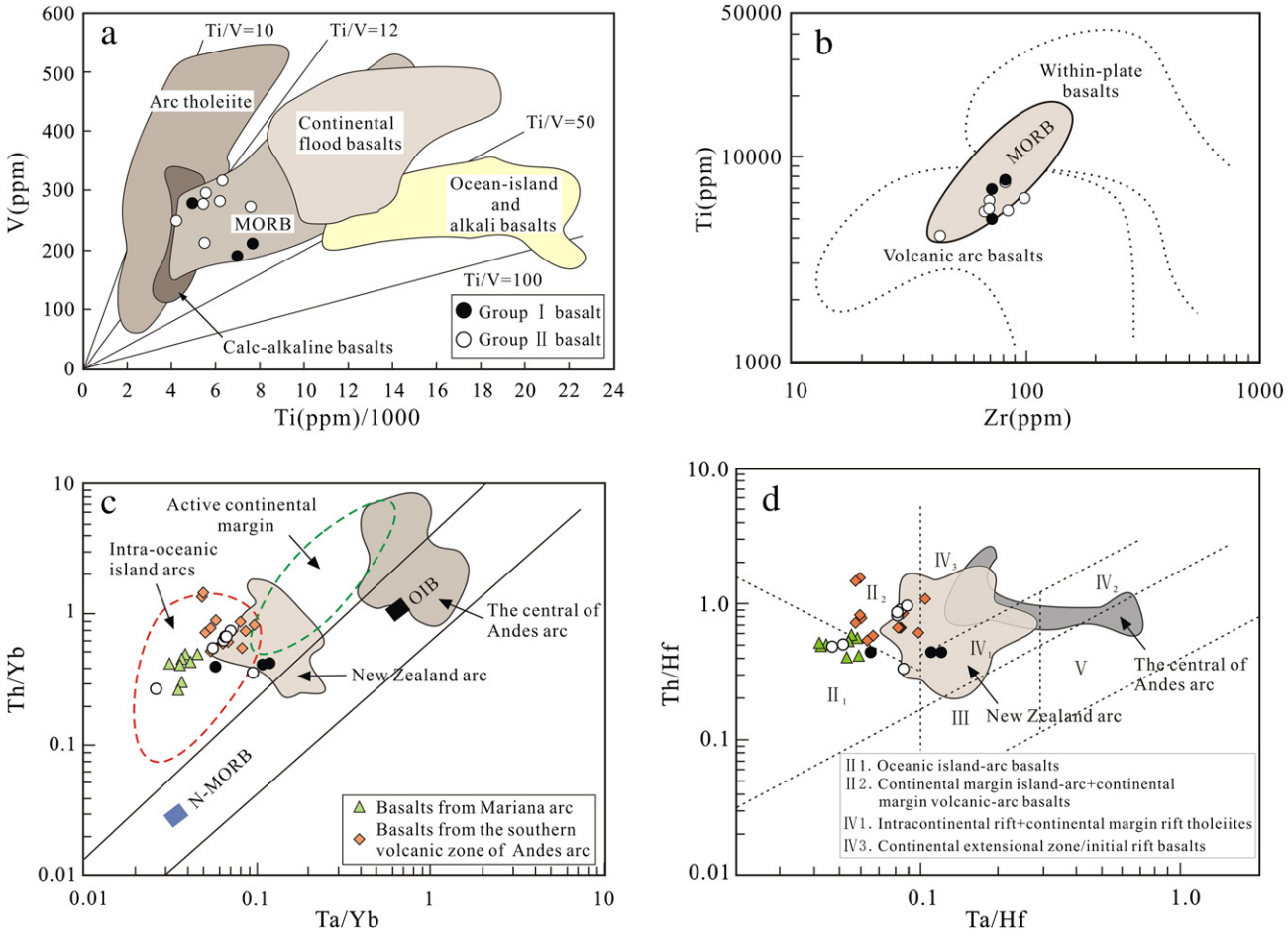

Fig. 10. Tectonic discrimination diagrams for Bima Formation basalts. (a) V vs. Ti diagram (after Shervais, 1982). The fields of arc tholeiite, calc-alkaline basalt, mid-ocean-ridge basalt (MORB), continental flood basalt, and ocean-island and alkali basalts were drawn by Rollinson (1993) according to Shervais (1982). (b) Ti vs. Zr diagram (after Pearce, 1982). (c) Th/Yb vs. Ta/Yb diagram (after Pearce, 1983). (d) Th/Hf vs. Ta/Hf diagram (after Wang et al., 2001). Data of New Zealand arc, Mariana arc, Central and Southern volcanic zone of Andes arc are all from http://georoc.mpch-mainz.gwdg.de/georoc/.

differences from typical continental margin arc basalts, such as the central volcanic zone (CVZ) of the Andes arc, but similar to basalts from some intra-oceanic arc settings (Wilson, 1989). However, in the chondrite-normalized REE diagram (Fig.6a), the Bima Formation basalts show light LREE enrichment, which is different from either the CVZ of the Andes arc that has a mature continental crust, or typical intra-oceanic arcs, such as the Marianas and the Tonga-Kermadec arcs (Peate and Pearce, 1998; Smith et al., 2010), but similar to basalts from the southern volcanic zone (SVZ) of the Andes arc and Zao volcano of northeastern Japan arc (with the exception of sample 10SR-23) (Tatsumi et al., 2008; Wilson, 1989), In Th/Yb vs. Ta/Yb and Th/Hf vs. Ta/Hf diagrams (Fig. 10c, d), we can get similar conclusion that the Bima Formation rocks are different from the rocks of Mariana arc (typical intra-oceanic arc) and CVZ (central Andes arc with mature and thick crust), however, they plot in the fields of New Zealand arc, SVZ, NVZ (southern and northern parts of Andes arc) and Japan arc (with thin crust). The $^{143}Nd/^{144}Nd$ vs. $^{86}Sr/^{87}Sr$ diagram (Fig. 11) shows that the Bima Formation basalts are less depleted than typical intra-oceanic arcs, such as the New Britain, Marianas, South Sandwich, and Aleutian arcs. Instead, they plot within the fields of Japanese, NVZ (the northern volcanic zone of the Andes arc), and Java arcs, indicating little crustal contamination. In summary, the Bima Formation basalts were most likely derived from a subduction zone covered by thin juvenile arc crust, which is consistent with the fact that the southern Lhasa Terrane had no mature crust during the Mesozoic (Ji et al., 2009; Zhu et al., 2011).

An intra-oceanic subduction system was recognized within the Yarlung-Zangbo suture zone (Aitchison et al., 2000; McDermid et al., 2002). This subduction system extended eastward into the area between India and Burma, and westward between India and Karakoram (Dai et al., 2013). In the Zedong region, southwest of our study area, Aitchison et al. (2007) identified a suite of intra-oceanic arc volcanic rocks. The question now is whether or not the Bima Formation volcanic rocks had any relationship with this intra-oceanic subduction system. Based on the data presented in this paper, it is also possible that the magmas of the Bima Formation volcanic rocks were generated in an oceanic arc setting. To better understand the tectonic setting of the Bima Formation volcanic rocks, further research on the sedimentary rocks associated with the volcanic rocks, their tectonic and sedimentary environment is needed.

5.3. Early Jurassic magmatism and its significance

The evolutionary history of the Neo-Tethys remains debatable. It was generally believed that the subduction of the Neo-Tethys began during the Cretaceous or during the Middle Jurassic. However, more and more Late Triassic-Early Jurassic felsic intrusions have recently been reported in the southern Lhasa Terrane (Chu et al., 2006; Guo et al., 2013; Ji et al., 2009; Qu et al., 2007; Tang et al., 2010; Yang et al., 2008; Zhang et al., 2007), and the majority of these intrusions show positive zircon $\varepsilon_{Hf}(t)$ and whole-rock $\varepsilon_{Nd}(t)$ features suggesting that they were generated from partial melting of juvenile crust possibly related to the northward subduction of the Neo-Tethys, so the subduction may began during the Late Triassic-Early Jurassic (Chu et al., 2006; Guo et al., 2013; Ji et al., 2009; Wu et al., 2010).

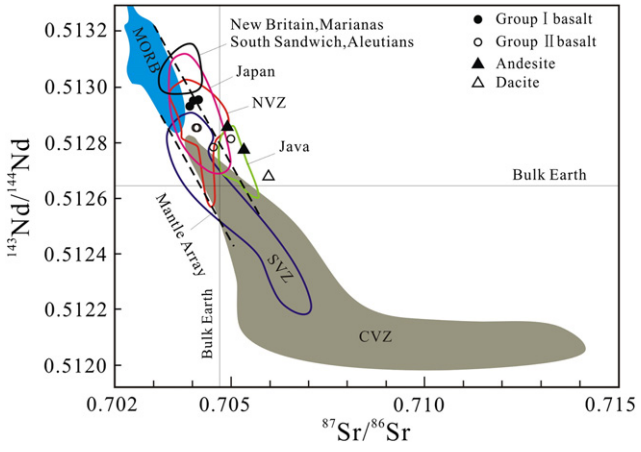

Fig. 11. $^{143}Nd/^{144}Nd$ vs. $^{87}Sr/^{86}Sr$ diagram for Bima Formation volcanic rocks (after Winter, 2010).

The sporadically distributed Yeba Formation volcanic rocks are the only well-researched Early Jurassic volcanic rocks in southern Lhasa subterrane so far (Dong et al., 2006; Zhu et al., 2008). They are distal from the Indus-Yarlung Zangbo suture zone and distribute only to the east of the Lhasa city, which is different from the Early Jurassic felsic intrusions (Guo et al., 2013). Accompanied by the Early Jurassic felsic intrusions, the presented volcanic rocks of the Sangri Group are located to the south of outcrops of the Yeba Formation and extend over 800 km. Ages of the volcanic rocks of the Bima Formation are from 195 to 189 Ma (we also obtained a zircon SHRIMP U-Pb age of 177 Ma from andesite to the northwest of the Xigaze city), identical to the ages (202-150 Ma) of detrital zircons of sediments of the Xigaze forearc basin, which is interpreted to be derived from the north Gangdese magmatic arc (Wu et al., 2010). In summary, the Bima Formation volcanic rocks of the Sangri Group serve as direct evidence for arc volcanism and for initial northward subduction of the Neo-Tethys along the southern Lhasa Terrane before 195 Ma. The Gangdese magmatic arc was initiated during Late Triassic-Early Jurassic times due to northward subduction of the Neo-Tethys, and experienced a relatively complicated history. Substantial erosion caused by Tibetan Plateau uplift since the Cretaceous may have removed most of the Early Jurassic volcanic rocks (Wu et al., 2010), leaving only a few remaining in place today.

6. Conclusions

Major conclusions are drawn based on the geochronological and geochemical analyses of the Bima Formation volcanics presented in this paper:

(1) We obtained the first zircon U-Pb ages from the Bima Formation volcanics, based on these new ages, and the published ages of the Mamuxia Formation volcanic rocks, the Bima Formation volcanic rocks are older than the Mamuxia Formation, contrary to what has been previously reported. Therefore, the stratigraphy of the Sangri Group volcano-sedimentary rocks needs to be reexamined.
(2) The Bima Formation volcanic rocks distributed around the Sangri County comprise dominantly intermediate-mafic rocks and are characterized by typical island arc volcanic geochemical features. The magmas were generated by northward subduction of the Neo-Tethys along the southern Lhasa Terrane during the Early Jurassic. The magmas were likely sourced from a MORB-like depleted mantle wedge that was metasomatized by subducted slab-derived fluids, and subsequently experienced juvenile crustal contamination and fractional crystallization of mafic minerals during ascent.
(3) The ages of the Bima Formation show that there was intense arc volcanism between 195 and 177 Ma, coeval with felsic intrusions along southern Lhasa Terrane, implying that the northward subduction of the Neo-Tethys had developed prior to 195 Ma.

Acknowledgments

This study was supported by the Strategic Priority Research Program(B)of the Chinese Academy of Sciences (Grant No. DB03010300), the National Natural Science Foundation of China (Grant No. 41003018), the Natural Science Foundation of Guangxi (Grant No. 2012GXNSFBA053132), and the Postdoctoral Science

Foundation. We thank Z. C. Hu for his help with LA-ICP-MS dating, and Y. Liu, G. Q. Hu, J. Li, and G. Q. Wang for their assistance with the major, trace, and isotope analysis, respectively.

References

Aitchison, J.C., Badengzhu, Davis, A.M., Liu, J.B., Luo, H., Malpas, J.G., McDermid, I.R.C., Wu, H.Y., Ziabrev, S.V., Zhou, M.F., 2000. Remnants of a Cretaceous intra-oceanic subduction system within the Yarlung-Zangbo suture(southern Tibet). Earth and Planetary Science Letters 183, 231–244.

Aitchison, J.C., Ali, J.R., Davis, A.M., 2007. When and where did India and Asia collide? Journal of Geophysical Research 112, B05423.

Anderson, T., 2002. Correction of common lead in U-Pb analyses that do not report ^{204}Pb. Chemical Geology 192, 59–79.

Ayers, J., 1998. Trace element modeling of aqueous fluid-peridotite interaction in the mantle wedge of subduction zones. Contributions to Mineralogy and Petrology 132, 390–404.

Bacon, C.R., Druitt, T.H., 1988. Compositional evolution of the zoned calc-alkaline magma chamber of Mount Mazama, Crater Lake, Oregon. Contributions to Mineralogy and Petrology 98, 224–256.

Bacon, C.R., Bruggman, P.E., Christiansen, R.L., Clynne, M.A., Donnelly-Nolan, J.M., Hildreth, W., 1997. Primitive magmas at five Cascade volcanic fields: melts from hot, heterogeneous sub-arc mantle. The Canadian Mineralogist 35, 397–423.

Barley, M.E., Pickard, A.L., Zaw, K., Rak, P., Doyle, M.G., 2003. Jurassic to Miocene magmatism and metamorphism in the Mogok metamorphic belt and the India-Eurasia collision in Myanmar. Tectonics. http://dx.doi.org/10.1029/2002TC001398.

Belousova, E.A., Griffin, W.L., O'Reilly, S.Y., Fisher, N.I., 2002. Igneogus zircon: trace element composition as an indicator of source rock type. Contributions to Mineralogy and Petrology 143, 602–622.

Ben Othman, D., White, W.M., Patchett, J., 1989. The geochemistry of marine sediments, island arc magma genesis, and crust-mantle recycling. Earth and Planetary Science Letters 94, 1–21.

Bienvenu, P., Bougault, H., Joron, M., Dmitriev, L., 1990. MORB alteration: rare-earth element/non-rare earth hygromagmaphile element fractionation. Chemical Geology 82, 1–14.

Bonin, B., 2004. Do coeval mafic and silicic magmas in post-collisional to within-plate regimes necessarily imply two contrasting, mantle and crustal, sources? Lithos 78 (1–2), 1–24.

Chen, J.S., Huang, B.C., Sun, L.S., 2010. New constraints to the onset of the India-Asia collision: Paleomagnetic reconnaissance on the Linzizong Group in the Lhasa Block, China. Tectonophysics 489 (1–4), 189–209.

Chen, Y., Zhu, D.C., Zhao, Z.D., Meng, F.Y., Wang, Q., Santosh, M., Wang, L.Q., Dong, G.C., Mo, X.X., 2013. Slab breakoff triggered ca. 113 Ma magmatism around Xainza area of the Lhasa Terrane, Tibet. Gondwana Research. http://dx.doi.org/10.1016/j.gr.2013.06.005.

Chu, M.F., Chung, S.L., Song, B., Liu, D.Y., O'Reilly, S.Y., Pearson, N.J., 2006. Zircon U-Pb and Hf isotope constraints on the Mesozoic tectonics and crustal evolution of southern Tibet. Geology 34 (9), 745–748.

Chung, S.L., Chu, M.F., Zhang, Y.Q., Xie, Y.W., Lo, C.H., Lee, T.Y., Lan, C.Y., Li, X.H., Zhang, Q., Wang, Y.Z., 2005. Tibetan tectonic evolution inferred from spatial and temporal variations in post-collisional magmatism. Earth-Science Reviews 68, 173–196.

Dai, J.G., Wang, C.S., Hébert, R., Santosh, M., Li, Y.L., Xu, J.Y., 2013. Petrology and geochemistry of peridorites in the Zhongba ophiolite, Yarlung Zangbo Suture Zone: Implications for the Early Cretaceous intra-oceanic subduction zone within the Neo-Tethys. Chemical Geology 288, 133–148.

DePaolo, D.J., 1988. Neodymium Isotope Geochemistry: An Introduction. Springer, New York p. 181.

Dewey, J.F., Shackleton, R.M., Chang, C.F., Sun, Y.Y., 1988. The tectonic evolution of the Tibetan Plateau. Philosophical Transactions of the Royal Society of London (Series A): Mathematical and Physical Sciences 327, 379–413.

Dong, Y.H., Xu, J.F., Zeng, Q.G., Wang, Q., Mao, G.Z., Li, J., 2006. Is there a Neo-Tethys' subduction record earlier than arc volcanic rocks in the Sangri Group? Acta Petrologica Sinica 22 (3), 661–668 (in Chinese with English abstract).

Frey, F.A., Green, D.H., Roy, S.D., 1978. Integrated models of basalt petrogenesis: a study of quartz tholeiites to olivine melilitites from South Eastern Australia utilizing geochemical and experimental petrological data. Journal of Petrology 19, 463–513.

Gertisser, R., Keller, J., 2003. Trace element and Sr, Nd, Pb and O isotope variations in medium-K and high-K volcanic rocks from Merapi volcano, central Java, Indonesia: evidence for the involvement of subducted sediments in Sunda arc magma genesis. Journal of Petrology 44, 457–489.

Guffanti, M., Clynne, M.A., Muffler, L.J.P., 1996. Thermal and mass implications of magmatic evolution in the Lassen volcanic region, California, and constraints on basalt influx to the lower crust. Journal of Geophysical Research 101, 3001–3013.

Guo, L.S., Liu, Y.L., Liu, S.W., Cawood, P.A., Wang, Z.H., Liu, H.F., 2013. Petrogenesis of early to middle Jurassic granitoid rocks from the Gangdese belt, Southern Tibet: implications for early history of the Neo-Tethys. Lithos 179, 320–333.

Guynn, J.H., Kapp, P., Pullen, A., Heizler, M., 2006. Tibetan basement rocks near Amdo reveal 'missing' Mesozoic tectonism along the Bangong suture, central Tibet. Geology 34 (6), 505–508.

He, S.D., Kapp, P., DeCelles, P.G., Gehrels, G.E., Heizler, M., 2007. Cretaceous-Tertiary geology of the Gangdese Arc in the Linzhou area, southern Tibet. Tectonophysics 433, 15–37.

Hess, P.C., 1992. Phase equilibria constraints on the origin of ocean floor basalts. In: Morgan, J.P., Blackman, D.K., Sinton, J.M. (Eds.), Mantle Flow and Melt Generation at Mid-Ocean Ridges. American Geophysical Union, Geophysical Monograph, 71, pp. 67–102.

Ji, W.Q., Wu, F.Y., Chung, S.L., Li, J.X., Liu, C.Z., 2009. Zircon U-Pb geochronology and Hf isotopic constraints on petrogenesis of the Gangdese batholith, southern Tibet. Chemical Geology 262, 229–245.

Kang, Z.Q., Xu, J.F., Chen, J.L., Wang, B.D., 2009. Geochemistry and origin of Cretaceous adakites in Mamuxia Formation, Sangri Group, South Tibet. Geochimica 38 (7), 334–344 (in Chinese with English abstract).

Kang, Z.Q., Xu, J.F., Chen, J.L., Wang, B.D., Dong, Y.H., 2010. The geochronology of Sangri Group volcanic rocks in Tibet: Constraints from later Mamen intrusions. Geochimica 39 (6), 520–530 (in Chinese with English abstract).

Kapp, P., DeCelles, P.G., Gehrels, G.E., Heizler, M., Ding, L., 2007. Geological records of the Lhasa-Qiangtang and Indo-Asian collisions in the Nima area of central Tibet. GSA Bulletin 119, 917–932.

Kimura, J.I., Yoshida, T., 2006. Contributions of slab fluid, mantle wedge and crust to the origin of quaternary lavas in the NE Japan arc. Journal of Petrology 47, 2185–2232.

La Flèche, M., Camire, G., Jenner, G., 1998. Geochemistry of post-Acadian, Carboniferous continental intraplate basalts from the Maritimes Basin, Magdalen islands, Quebec, Canada. Chemical Geology 148, 115–136.

Leat, P.T., Riley, T.R., Wareham, C.D., Millar, I.L., Kelley, S.P., Storey, B.C., 2002. Tectonic setting of primitive magmas in volcanic arcs: An example from the Antarctic Peninsula. Journal of the Geological Society 159, 31–44.

Lee, H.Y., Chung, S.L., Wang, Y.B., Zhu, D.C., Yang, J.S., Song, B., Liu, D.Y., Wu, F.Y., 2007. Age, petrogenesis and geological significance of the Linzizong volcanic successions in the Linzhou basin, southern Tibet: evidence from zircon U-Pb dates and Hf isotopes. Acta Petrologica Sinica 23 (2), 493–500 (in Chinese with English abstract).

Lee, H.Y., Chung, S.L., Ji, W.Q., Gallet, S., Lo, C.H., Lee, T.Y., Zhang, Q., 2012. Geochemical and Sr-Nd isotopic constraints on the genesis of the Cenozoic Linzizong volcanic successions, southern Tibet. Journal of Asian Earth Sciences 53 (7), 96–114.

Li, X.H., Qi, C.S., Liu, Y., Liang, X.R., Tu, X.L., Xie, L.W., Yang, Y.H., 2005. Petrogenesis of the Neoproterozoic bimodal volcanic rocks along the western margin of the Yangtze block: New constraints from Hf isotopes and Fe/Mn ratios. Chinese Science Bulletin 50, 2481–2486.

Liang, X.R., Wei, G.J., Li, X.H., Liu, Y., 2003. Precise measurement of ^{143}Nd/^{144}Nd and Sm/Nd ratios using multiple-collectors inductively couple plasma-mass spectrometer (MC-ICP-MS). Geochimica 32, 91–96 (in Chinese with English abstract).

Liu, Y., Liu, H.C., Li, X.H., 1996. Simultaneous and precise determination of 40 trace elements in rock samples using ICP-MS. Geochimica 25 (6), 552–558 (in Chinese with English abstract).

Liu, Y.S., Hu, Z.C., Gao, S., Gunther, D., Xu, J., Gao, C.G., Chen, H.H., 2008. In situ analysis of major and trace elements of anhydrous minerals by LA-ICP-MS without applying an internal standard. Chemical Geology 257 (1–2), 34–43.

Liu, Y.S., Hu, Z.C., Zong, K.Q., Gao, C.G., Gao, S., Xu, J.A., Chen, H.H., 2010. Reappraisement and refinement of zircon U-Pb isotope and trace element analyses by LA-ICP-MS. Chinese Science Bulletin 55, 1535–1546.

Ludwig, K.R., 2003. ISOPLOT 3.00: A Geochronological Toolkit for Microsoft Excel. Berkeley Geochronology Center, California, Berkeley p. 39.

Ma, L., Wang, Q., Li, Z.X., Wyman, D.A., Jiang, Z.Q., Yang, J.H., Gou, G.N., Guo, H.F., 2013a. Early late Cretaceous (ca. 93 Ma) norites and hornblendites in the Milin area eastern Gangdese: Lithosphere-asthenosphere interaction during slab roll-back and an insight into early late Cretaceous (ca. 100-80 Ma) magmatic 'flare-up' in southern Lhasa (Tibet). Lithos 172–173, 17–30.

Ma, L., Wang, Q., Li, Z.X., Wyman, D.A., Jiang, Z.Q., Yang, J.H., Li, Q.L., Gou, G.N., Guo, H.F., 2013b. Late Cretaceous crustal growth in the Gangdese area, southern Tibet: Petrological and Sr-Nd-Hf-O isotopic evidence from Zhengga diorite-gabbro. Chemical Geology 349–350, 54–70.

Mahoney, J.J., Frei, R., Tejada, M., Mo, X., Leat, P., Nägler, T., 1998. Tracing the Indian Ocean mantle domain through time: isotopic results from old West Indian, East Tethyan, and South Pacific seafloor. Journal of Petrology 39, 1285–1306.

McDermid, I.R.C., Aitchison, J.C., Davis, A.M., Harrison, T.M., Grove, M., 2002. The Zedong terrane: a Late Jurassic intra-oceanic magmatic arc within the Yarlung-Tsangpo suture zone, southeastern Tibet. Chemical Geology 187, 267–277.

Miyashiro, A., 1974. Volcanic rock series in island arcs and active continental margins. American Journal of Science 274, 321–355.

Mo, X.X., Zhao, Z.D., Deng, J.F., Dong, G.C., Zhou, S., Guo, T.Y., Zhang, S.Q., Wang, L.L., 2003. Response of volcanism to the India-Asia collision. Earth Science Frontiers (Chinese University of Geoscience, Beijing) 10, 135–148 (in Chinese with English abstract).

Mo, X.X., Dong, G.C., Zhao, Z.D., Guo, T.Y., Wang, L.L., Chen, T., 2005a. Timing of magma mixing in Gangdese magmatic belt during the India-Asia collision: zircon SHRIMP U-Pb dating. Acta Geologica Sinica 79, 66–76.

Mo, X.X., Dong, G.C., Zhao, Z.D., Zhou, S., Wang, L.L., Qiu, R.Z., Zhang, F.Q., 2005b. Spatial and temporal distribution and characteristics of granitoids in the Gangdese, Tibet and implication for crustal growth and evolution. Geological Journal of China Universities 11, 281–290 (in Chinese with English abstract).

Mo, X.X., Hou, Z.Q., Niu, Y.L., Dong, G.C., Qu, X.M., Zhao, Z.D., Yang, Z.M., 2007. Mantle contributions to crustal thickening during continental collision: evidence from Cenozoic igneous rocks in southern Tibet. Lithos 96, 225–242.

Mo, X.X., Niu, Y.L., Dong, G.C., Zhao, Z.D., Hou, Z.Q., Zhou, S., Ke, S., 2008. Contribution of syncollisional felsic magmatism to continental crust growth: a case study of the Paleocene Linzizong Volcanic Succession in southern Tibet. Chemical Geology 250, 49–67.

Morra, V., Secchi, F.A.G., Melluso, L., Franciosi, L., 1997. High-Mg subduction-related tertiary basalts in Sardinia, Italy. Lithos 40, 69–91.

Pan, Y.S., Fang, A.M., 2010. Formation and evolution of the Tethys in the Tibetan Plateau. Chinese Journal of Geology 45 (1), 92–101 (in Chinese with English abstract).

Pearce, J.A., 1982. In: Thorpe, R.S. (Ed.), Trace element characteristics of lavas from destructive plate boundaries Andesites. Wiley, Chichester, pp. 525–548.

Pearce, J.A., 1983. Role of the sub-continental lithosphere in magma genesis at active continental margins. In: Hawkesworth, C.J., Norry, M.J. (Eds.), Continental Basalts and Mantle Xenoliths. Shiva Publishing Nantwich, pp. 158–185.
Pearce, J.A., Cann, J.R., 1973. Tectonic setting of basic volcanic rocks determined using trace element analyses. Earth and Planetary Science Letters 19, 290–300.
Pearce, J.A., Norry, M.J., 1979. Petrogenetic implications of Ti, Zr, Y and Nb variations in volcanic rocks. Contributions to Mineralogy and Petrology 69, 33–47.
Peate, D.W., Pearce, J.A., 1998. Causes of spatial compositional variations in Mariana arc lavas: Trace element evidence. The Island Arc 7, 479–495.
Peng, T.P., Wang, Y.J., Zhao, G.C., Fan, W.M., Peng, B.X., 2008. Arc-like volcanic rocks from the southern Lancangjiang zone, SW China: Geochronological and geochemical constraints on their petrogenesis and tectonic implications. Lithos 102, 358–373.
Perfit, M.R., Gust, D.A., Bence, A.E., Arculus, R.J., Taylor, S.R., 1980. Chemical characteristics of island-arc basalts: implications for mantle sources. Chemical Geology 30, 227–256.
Petrone, C.M., Francalanci, L., Carlson, R.W., Ferrari, L., Conticelli, S., 2003. Unusual coexistence of subduction-related and intraplate-type magmatism: Sr, Nd and Pb isotope and trace element data from the magmatism of the San Pedro-Ceboruco graben Nayarit, Mexico. Chemical Geology 193, 1–24.
Pin, C., Paquette, J.L., 1997. A mantle-derived bimodal suite in the Hercynian belt: Nd isotope and trace element evidence for a subduction-related rift origin of the late Devonian Brevenne metavolcanics, Massif Central (France). Contributions to Mineralogy and Petrology 129, 222–238.
Plank, T., Langmuir, C.H., 1998. The chemical composition of subducting sediment and its consequences for the crust and mantle. Chemical Geology 145, 325–394.
Qu, X.M., Xin, H.B., Xu, W.Y., 2007. Collation of age of ore-hosting volcanics in Xiongcun superlarge Cu-Au deposit on basis of three zircon U-Pb SHRIMP ages. Mineral Deposits 26 (5), 512–518 (in Chinese with English abstract).
Riley, T.R., Leat, P.T., Pankhurst, R.J., Harris, C., 2001. Origins of large volume rhyolitic volcanism in the Antarctic Peninsula and Patagonia by crust melting. Journal of Petrology 42, 1043–1065.
Roberts, M.P., Clemens, J.D., 1993. Origin of high-potassium, calc-alkaline, I-type granitoids. Geology 21, 825–828.
Rollinson, H.R., 1993. Using Geochemical Data: Evaluation, Presentation, Interpretation: London, Longman Geochemistry Society. pp. 184–186.
Rowley, D.B., 1996. Age of initiation of collision between India and Asia: a review of stratigraphic data. Earth and Planetary Science Letters 145, 1–13.
Schärer, U., Xu, R.H., Allègre, C.J., 1984. U-Pb geochronology of Gandese (Transhimalaya) plutonism in the Lhasa-Xigaze region Tibet. Earth and Planetary Science Letters 69, 311–320.
Searle, M.P., Kahn, M.A., Fraser, J.E., Gough, S.J., 1999. The tectonic evolution of the Kohistan-Karakoram collision belt along the Karakoram Highway transect, north Pakistan. Tectonics 18, 929–949.
Searle, M.P., Noble, S.R., Cottle, J.M., Waters, D.J., Mitchell, A.H.G., Hlaing, T., Horstwood, M.S.A., 2007. Tectonic evolution of the Mogok metamorphic belt, Burma (Myanmar) constrained by U-Th-Pb dating of metamorphic and magmatic rocks. Tectonics 26, TC3014.
Seghedi, I., Downes, H., Pécskay, Z., Thirlwall, M., Szakács, A., Prychodko, M., Mattey, D., 2001. Magma genesis in a subduction-related post-collisional volcanicarc segment: the Ukrainian Carpathians. Lithos 57, 237–262.
Sengör, A.M.C., 1979. Mid-Mesozoic closure of Permo-Triassic Tethys and its implications. Nature 279, 590–593.
Shervais, J.W., 1982. Ti-V plots and the petrogenesis of modern and ophiolitic lavas. Earth and Planetary Science Letters 59, 101–118.
Smith, I.E.M., Stewart, R.B., Price, R.C., Worthington, T.J., 2010. Are arc-type rocks the products of magma crystallization? Observation from a simple oceanic arc volcano: Raoul Island, Kermadec Arc, SW Pacific. Jornal of Volcanology and Geothermal Research 190, 219–234.
Staudigel, H., Plank, T., White, B., Schmincke, H.U., 1996. Geochemical fluxes during seafloor alteration of the basaltic upper oceanic crust: DSDP sites 417 and 418, 19-38. In: Bebout, G.E., Scholl, S.W., Kirby, S.H., Platt, J.P. (Eds.), American Geophysical Union, Washington, DC.
Stolz, A.J., Vame, R., Wheller, G.E., Foden, J.D., Abbott, M.J., 1988. The geochemistry and petrogenesis of K-rich alkaline volcanics from the Batu Tara volcano, eastern Sunda Arc. Contributions to Mineralogy and Petrology 98, 374–389.
Stolz, A.J., Vame, R., Davies, G.R., Wheller, G.E., Foden, J.D., 1990. Magma source components in an arc-continent collision zone: the Flores-Lembata sector, Sunda Arc, Indonesia. Contributions to Mineralogy and Petrology 105, 585–601.
Sui, Q.L., Wang, Q., Zhu, D.C., Zhao, Z.D., Chen, Y., Santosh, M., Hu, Z.C., Yuan, H.L., Mo, X.X., 2013. Compositional diversity of ca.110 Ma magmatism in the northern Lhasa Terrane, Tibet: Implications for the magmatic origin and crustal growth in a continent-continent collision zone. Lithos 168-169, 144–159.
Sun, S.S., McDonough, W.F., 1989. In: Saunders, A.D. (Ed.), Chemical and Isotope Systematics of Oceanic Basalts: Implications for Mantle Composition and Processes. Magmatism in ocean Basins, 42. Geological Society Publication, pp. 313–345.
Takahashi, T., Hirahara, Y., Miyazaki, T., Senda, R., Chang, Q., Kimura, J.I., Tatsumi, Y., 2013. Primary magmas at the volcanic front of the NE Japan arc: Coeval eruption of crustal low-k tholeiitic and mantle-derived medium-k calc-alkaline basalts at Azuma volcano. Journal of Petrology 54 (1), 103–148.
Tang, J.X., Li, F.J., Li, Z.J., Zhang, L., Tang, X.Q., Deng, Q., Lang, X.H., Huang, Y., Yao, X.F., Yao, X.F., Wang, Y., 2010. Time limit for formation of main geological bodies in Xiongcun copper-gold deposit, Xietongmen County, Tibet: evidence from zircon U-Pb ages and Re-Os age of molybdenite. Mineral Deposits 29 (3), 461–475 (in Chinese with English abstract).
Tatsumi, Y., Kogiso, T., 1997. Trace element transport during dehydration processes in the subducted oceanic crust: 2. Origin of chemical and physical characteristics in arc magmatism. Earth and Planetary Science Letters 148, 207–221.
Tatsumi, Y., Takahashi, T., Hirahara, Y., Chang, Q., Miyazaki, T., Kimura, J.I., Ban, M., Sakayori, A., 2008. New insights into Andesite genesis: the role of mantle-derived calc-alkalic and crust-derived tholeiitic melts in magma differentiation beneath Zao volcano, NE Japan. Journal of Petrology 49 (11), 1971–2008.
Tepper, J.H., Nelson, B.K., Bergantz, G.W., Irving, A.J., 1993. Petrology of the Chilliwack batholith, North Cascades, Washington: generation of calc-alkaline granitoids by melting of mafic lower crust with variable water fugacity. Contributions to Mineralogy and Petrology 113, 333–351.
Vroon, P.Z., van Bergen, M.J., White, W.M., Varekamp, J.C., 1993. Sr-Nd-Pb isotope systematics of the Banda arc, Indonesia: combined subduction and assimilation of continental material. Journal of Geophysical Research 98, 22349–22366.
Vroon, P.Z., van Bergen, M.J., Klaver, G.J., White, W.M., 1995. Strontium, neodymium, and lead isotopic and trace-element signature of the East Indonesian sediments: provenance and implications for Banda Arc magma genesis. Geochemica et Cosmochimica Acta 59, 2573–2598.
Wang, Y.L., Zhang, C.J., Xiu, S.Z., 2001. Th/Hf-Ta/Hf identification of tectonic setting of basalts. Acta Petrologica Sinica 17, 413–421 (in Chinese with English abstract).
Wen, D.R., Liu, D.Y., Chung, S.L., Chu, M.F., Ji, J.Q., Zhang, Q., Song, B., Lee, T.Y., Yeh, M.W., Lo, C.H., 2008. Zircon SHRIMP U-Pb ages of the Gangdese Batholith and implications for Neo-Tethyan subduction in southern Tibet. Chemical Geology 252, 191–201.
Wilson, M., 1989. Igneous petrogenesis: a global tectonic approach. Unwin Hyman, London (Chapter 6-7).
Winchester, J.A., Floyd, P.A., 1976. Geochemical magma type discrimination: Application to altered and metamorphosed basic igneous rocks. Earth and Planetary Science Letters 28, 459–469.
Winter, J.D., 2010. Principles of Igneous and Metamorphic Petrology, Second edition. Prentice Hall, New Jersey (Chapter 16-17).
Wu, Y.B., Zheng, Y.F., 2004. Study on genesis of zircon and its constrains on interpretation of U-Pb age. Chinese Science Bulletin 49, 1589–1604 (in Chinese with English abstract).
Wu, F.Y., Ji, W.Q., Liu, C.Z., Chung, S.L., 2010. Detrital zircon U-Pb and Hf isotopic data from the Xigaze fore-arc basin: constraints on Transhimalayan magmatic evolution in southern Tibet. Chemical Geology 271, 13–25.
Xia, D.X., Liu, S.K., 1997. Lithostratigraphy of Xizang Autonomous Region [M]. China University of Geosciences Press, Wuhan pp. 1–200 (in Chinese).
Xu, J.F., Castillo, P.R., 2004. Geochemical and Nd-Pb isotopic characteristics of the Tethyan asthenosphere: implications for the origin of the Indian Ocean mantle domain. Tectonophysics 393, 9–27.
Yalew, D., Yirgu, G., 2003. Crustal contribution to the genesis of Ethiopian plateau rhyolitic ignimbrites: basalt and rhyolite geochemical provinciality. Journal of the Geological Society 160, 47–56.
Yang, Z.M., Hou, Z.Q., Xia, D.X., Song, Y.C., Li, Z., 2008. Relationship between western porphyry and mineralization in Qulong copper deposit of Tibet and its enlightenment to further exploration. Mineral Deposits 27, 28–36 (in Chinese with English abstract).
Yin, A., Harrison, T.M., 2000. Geologic evolution of the Himalayan-Tibetan orogen. Annual Review of Earth and Planetary Sciences 28, 211–280.
Zhang, S.Q., Mahoney, J., Mo, X.X., Ghazi, A., Milani, L., Crawford, A., Guo, T.Y., Zhao, Z.D., 2005. Evidence for a widespread Tethyan upper mantle with Indian-Ocean-type isotopic characteristics. Journal of Petrology 46, 829–858.
Zhang, H.F., Xu, W.C., Guo, J.Q., Zong, K.Q., Cai, H.M., Yuan, H.L., 2007. Zircon U-Pb and Hf isotopic composition of deformed granite in the southern margin of the Gangdese Belt, Tibet: evidence for early Jurassic subduction of Neo-Tethyanoceanic slab. Acta Petrologica Sinica 23 (6), 1347–1353 (in Chinese with English abstract).
Zhu, J., Liu, Z.X., Zhang, H.J., Tian, W.X., Li, X.W., Tan, M.T., Li, Z.H., Gong, Z.Y., 2003. 1: 250,000 geological report of Lazi region with geological map. Institute of Hubei Geological Survey, Wuhan, unpublished (in Chinese).
Zhu, D.C., Pan, G., Mo, X., Liao, Z., Jiang, X., Wang, L., Zhao, Z., 2007. Petrogenesis of volcanic rocks in the Sangxiu Formation, central segment of Tethyan Himalaya: a probable example of plume-lithosphere interaction. Journal of Asian Earth Sciences 29, 320–335.
Zhu, D.C., Pan, G.T., Chung, S.L., Liao, Z.L., Wang, L.Q., Li, G.M., 2008. SHRIMP zircon age and geochemical constraints on the origin of lower Jurassic volcanic rocks from the Yeba Formation, Southern Gangdese, South Tibet. International Geology Review 50, 442–471.
Zhu, D.C., Zhao, Z.D., Pan, G.T., Lee, H.Y., Kang, Z.Q., Liao, Z.L., Wang, L.Q., Li, G.M., Dong, G.C., Liu, B., 2009. Early cretaceous subduction-related adakite-like rocks of the Gangdese Belt, southern Tibet: products of slabmelting and subsequentmelt-peridotite interaction? Journal of Asian Earth Sciences 34, 298–309.
Zhu, D.C., Zhao, Z.D., Niu, Y.L., Mo, X.X., Chung, S.L., Hou, Z.Q., Wang, L.Q., Wu, F.Y., 2011. The Lhasa Terrane: record of a micro continent and its histories of drift and growth. Earth and Planetary Science Letters 301, 241–255.
Zhu, D.C., Zhao, Z.D., Niu, Y.L., Dilek, Y., Wang, Q., Ji, W.H., Dong, G.C., Sui, Q.L., Liu, Y.S., Yuan, H.L., Mo, X.X., 2012. Cambrian bimodal volcanism in the Lhasa Terrane, southern Tibet: record of an early Paleozoic Andean-typemagmatic arc in the Australian proto-Tethyan margin. Chemical Geology 328, 290–308.
Zhu, D.C., Zhao, Z.D., Niu, Y.L., Dilek, Y., Hou, Z.Q., Mo, X.X., 2013. The origin and pre-Cenozoic evolution of the Tibetan Plateau. Gondwana Research 23 (4), 1429–1454.